DTU Library

An investigation and multi-criteria optimization of an innovative compressed air energy storage

Nabat, Mohammad Hossein; Habibzadeh, Mehran; Alsagri, Ali Sulaiman; Arabkoohsar, Ahmad

Published in:
Journal of Energy Storage

Link to article, DOI:
10.1016/j.est.2023.109645

Publication date:
2024

Document Version
Publisher's PDF, also known as Version of record

Journal of Energy Storage 76 (2024) 109645

Contents lists available at ScienceDirect

Journal of Energy Storage

journal homepage: www.elsevier.com/locate/est

Research papers

An investigation and multi-criteria optimization of an innovative compressed air energy storage

Mohammad Hossein Nabat [a,1], Mehran Habibzadeh [b,1], Ali Sulaiman Alsagri [c], Ahmad Arabkoohsar [a,*]

[a] Department of Civil and Mechanical Engineering, Technical University of Denmark, Kgs Lyngby, Denmark
[b] Department of Mechanical Engineering, University of Maine, Orono, ME 04469, USA
[c] Department of Mechanical Engineering, College of Engineering, Qassim University, Saudi Arabia

ARTICLE INFO

Keywords:
Compressed air energy storage
Constant-pressure air tank
Multi-objective optimization
Waste heat recovery
4E analyses

ABSTRACT

Compressed air energy storage, a well-known technique for energy storage purposes on a large scale, has recently attracted substantial interest due to the development and long-term viability of smart grids. The current research focus on the design and thorough examination of a compressed air energy storage system utilizing a constant pressure tank. Various aspects, including energy, exergy, economic, and exergoeconomic factors, have been extensively investigated in this study. The goal of the referenced design is to maximize the utilization of air's energy stored in the tank, minimize exergy destruction, enhance production capacity and energy storage density, optimize system performance, and recover waste heat efficiently. Additionally, through the utilization of artificial neural networks and genetic algorithms, this study provides an analysis of optimal operational conditions, taking into account both thermodynamic and economic performance considerations. The referenced system, which stores 209 MWh of excess power from the grid as compressed air and heat throughout off-peak times and utilizes it to produce 137 MWh of electrical power during peak demand periods, demonstrates remarkable performance compared to the conventional storage methods. The findings indicate that the total electrical efficiency, round trip efficiency, and exergy round trip efficiency of the referenced system are equal to 65.63 %, 68.28 %, and 66.01 %, respectively. The total cost of the products of the system is 21.15 $/GJ, while exhibiting a value of 190.4 $/MWh for its levelized cost of electricity. The system's payback period is approximately 5.11 years, and the ultimate profit amounts to around $40 million.

1. Introduction

To address the challenge of global warming, most of the governments have pledged to phase out fossil fuel power plants entirely within the coming decade, with the aim of sourcing the necessary energy from renewable resources [1]. The International Energy Agency (IEA) has predicted that the world's energy production capacity from renewable sources will be equal to the amount of electricity produced in fossil-fueled coal and gas plants by 2040 [2]. However, the intermittent nature of sustainable energy sources, such as wind and solar power, has resulted in a reduction in the reliability and expeditious integration of these sources into the energy markets [3]. Energy storage technologies on grid scales are considered an important and practical technique to tackle the mentioned problems [4]. Energy storage systems are able to store electrical energy produced by renewable resources in different ways, such as internal energy, potential or mechanical energy. During high-demand periods, the stored energy is converted into electrical power and delivered to the distribution network [5]. These systems can change the load distribution in the grid according to needs, prevent the generation and emission of greenhouse gases, and also provide black starts, standby power, frequency modulation, demand response support and other different offerings to the grid operation [6]. In this regard, energy storage techniques, which are crucial for smart grids have become the focus of research in the field of energy [7]. Grid-scale energy storage technologies include pumped storage, liquid air energy storage (LAES), compressed air energy storage (CAES), and hydrogen energy storage (HES) [8]. With the help of man-made tanks, CAES provides the benefits of extended life, high safety, cheap cost, quick reaction time, and freedom from environmental limitations when compared to other

* Corresponding author.
E-mail addresses: mh_nabat@yahoo.com, mhona@dtu.dk (M.H. Nabat), ahmar@dtu.dk (A. Arabkoohsar).
[1] These authors have equal contributions to the paper.

https://doi.org/10.1016/j.est.2023.109645
Received 21 July 2023; Received in revised form 23 October 2023; Accepted 9 November 2023

Nomenclature

A	Area [m^2]
c	Cost per unit of exergy [\$/GJ]
$\dot{C}$	Cost rate of streams [\$/h]
cp	Cost of products [\$/GJ]
$\$K$	Thousand dollars
$\$M$	Million dollars
ex_i	Specific exergy of each stream [kJ/kg]
$\dot{E}x$	Exergy rate [kW]
Ex_d	Exergy destruction [MWh]
$\dot{E}x_d$	Destruction rate of exergy [MW]
h	Specific enthalpy [kJ/kg]
h_x	Specific enthalpy at point x [kJ/kg]
hr/hrs	Hour(s)
i	Interest rate [%]
m	Mass [ton]
$\dot{m}$	Rate of mass flow [kg/s]
$\dot{m}_x$	Rate of mass flow at point x [kg/s]
n	Service lifetime of the system [year]
P_x	Pressure at point x [bar]
$\dot{Q}$	Rate of heat transfer [kW]
R^2	Coefficient of Determination [−]
s	Specific entropy [kJ/kg. K]
s_x	Specific entropy at point x [kJ/kg. K]
t	Time [hr]
T_x	Temperature at point x [°C]
V_i	Volume of the component i [m^3]
$\dot{W}$	Consumption /generation of power [kW]
Y_t	Net cost [\$]
yr	Year
Z	Cost [\$]
$\dot{Z}$	Cost rate [\$/hr]
ZT	Figure of merit [−]

Abbreviations

AC	Air compressor
ANN	Artificial neural network
ARC	Absorption refrigeration cycle
ASED	Air storage energy density [MJ/m^3]
AT	Air turbine
ATP	Annual total profit
C	Cooler
CAES	Compressed air energy storage
CAV	Compressed air vessel
COT	Cold oil tank
CP − CAES	Constant pressure compressed air energy storage
CRF	Capital recovery factor
ODP	Ozone depletion potential
Imp	Electrical efficiency improvement
Eco	Economizer
ERTE	Exergy round trip efficiency [%]
Evap	Evaporator
Gen	Generator
GWP	Global warming potential
HOT	Hot oil tank
HTES	High-temperature energy storage
HHX	Heating heat exchanger
HT	Hydraulic turbine
IHX	Internal heat exchanger
LAES	Liquid air energy storage
LCOE	Levelized cost of electricity
Mot	Electric-Motor
Mix	Mixer
NPV	Net present value
OP	ORC pump
ORC	Organic Rankine cycle
TSED	Total space energy density [MJ/m^3]
TIC	Total investment cost
OT	Oil tank
PHES	Pumped hydro energy storage
P	Pump
PT	Propane tank
Rec	Recuperator
RTE	Round trip efficiency [%]
SH	Superheater
ST	Steam turbine
TEG	Thermoelectric generation
TOPSIS	Technique for order of preference by similarity to the ideal solution
UW − CAES	Under water compressed air energy storage
WHR	Waste heat recovery
WP	Water pump

Subscripts

0	Dead condition
amb	Ambient
ch	Charge
chm	Chemical
dch	Discharge
elec	Electrical
env	Environmental
i	Stream
in	Inlet
k	Component
n	N-type
out	Outlet
p	P-type
phs	Physical
Q	Heat
s	Isentropic
W	Work
y	Year

Greek symbols

α	Seebeck coefficient [V/K]
η	Efficiency [%]
k	Total thermal conductivity [W/cm.K]
φ	Maintenance factor [−]
ρ	Density [kg/m^3]
σ	Electrical resistivity [Ω·cm]
τ	Yearly working hours of each component [hr]

energy storage systems now available [9].

The majority of proposed CAES systems in recent years have employed a constant volume tank for the storage of compressed air. In these configurations, the storage volume remains consistent while the storage pressure varies during both the charging and discharging phases. It should be noted that the utilization of a regulator to manage the discharge pressure in these constant volume systems has been associated with adverse impacts on system performance. According to the study by Razmi et al. [10], the largest share of exergy destruction in CAES systems with a constant volume tank associates with the regulator, which causes a huge part of the stored energy to be wasted. Also, in these systems, a part of the compressed air stored in the tank always remains intact, which causes dead volume in the storage tank. In light of this, recent studies have advocated for the adoption of constant pressure tanks due to their numerous advantages. The benefits of using constant pressure tank include [11,12]:

- The pressure during both the charging and discharging processes consistently matches, thereby leading to a higher power production in comparison to systems utilizing a constant volume tank.
- A constant pressure tank enables the system to fully release all the stored air, effectively reducing the storage volume.

Two primary approaches, including volatile fluids and underwater tanks, have been proposed for constant pressure tanks. Notably, the underwater compressed air storage system (UW-CAES) has emerged as a prominent innovation in recent years. In this method, air storage tanks are placed in the deep sea and the pressure of the tank is controlled by the hydrostatic pressure in the deep sea. The studies conducted in this field showed the significant advantage of this energy storage technology in energy and exergy efficiencies. The first pilot underwater storage tank system with a capacity of 750 kWh (1.5 MWh) was launched in 2014 by Hydrostor Corp at a depth of 80 m in Lake Ontario. Ebrahimi et al. [13] conducted a sophisticated exergy investigation on the UW-CAES system installed in Toronto. The results of their study show that 76.4 % of destruction of exergy is avoidable and 26.6 % is unavoidable, which indicates that the power plant has a good potential for performance improvement. Wang et al. [14] carried out an advanced exergy study on a UW-CAES system with a capacity of 2 MW and showed that the exergy efficiency of the proposed system in actual and ideal conditions is 53.6 % and 84.3 %, correspondingly. Zhao et al. [15] proposed a low-capacity UW-CAES system equipped with a humidifier-dehumidifier to supply drinking water to coastal areas. Their studies show that this system can produce 224.35 kWh with an electrical efficiency of 32.61 % during the discharge process. It also produces 851.77 kg of fresh water during the charging and discharging processes. Liu et al. [16] suggested a three-generation UW-CAES system combined with an ejector refrigeration cycle to increase system's products. The findings indicate that the total exergy efficiency of the suggested system in optimal condition is 55.85 % and the total investment cost is $296,288. Guo et al. [17] investigated the functionality of a UW-CAES system equipped with a floating tank and showed that the minimum pressure of the tank should be 30 bar, and the system's capacity for storing energy was 26.07 MJ/m^3 and the overall system performance was 70.74 %. Wang et al. [18] proposed a multilevel UW-CAES system and showed that the exergy efficiency can vary between 62 % and 81 %. However, within UW-CAES systems, the storage pressure is contingent upon the depth of the surrounding sea or lake, a condition that is not universally accessible across all regions of the world. Consequently, this limitation imposes noteworthy geographical and storage pressure constraints.

The use of volatile and condensable fluids like CO_2, hydrocarbon refrigerants, synthetic refrigerants, etc. is the second way of storing compressed air at constant pressure. Through proficient control of heat transfer processes, it is possible to manipulate the phase and pressure of volatile and condensable fluids, thus ensuring the maintenance of stored compressed air at the desired pressure. Chen et al. [19] proposed a new system using volatile fluids in a compressed air storage tank. They used CO_2/HC-600 with a ratio of 0.15/0.85 as volatile fluid in the tank and showed that the round-trip efficiency (RTE) value of the suggested system improved by 6.26 %. Chen et al. [20] continued their previous work and proposed two different configurations and showed that the exergy efficiency of the proposed system increases by 3 % in comparison to the CAES system with a constant volume reservoir. Rolland et al. [21] proposed pressure equalizing modules containing condensable gas to control pressure in constant pressure tanks. Considering qualitative (e.g., toxicity) and quantitative (e.g., molar mass) properties, they used R-1234ze(E) as phase change material inside the module and tested its effect in a power plant examined on a laboratory scale. Their results show that the capability to store of the experimental system has raised by 37.9 %, but the phase change is not completely constant pressure and temperature variations at the time of phase transition, prevent constant pressure storage. In the new proposed method based on volatile fluids, the storage pressure depends on the thermodynamic properties of volatile fluids, and it is not possible to store compressed air at high pressure. Therefore, the storage pressure is accompanied by limitations and this issue also affects the storage volume of the system, because with the increase of the storage pressure, the storage volume decreases significantly. Zhang et al. [2] proposed an adiabatic compressed air energy storage system with a pressure regulation inverter-driven compressor. Their studies show that such a system can improve round-trip efficiency by approximately 1.8–2.7 %, reducing the electricity balance cost by 0.57–0.85¢/kWh. In order to control the pressure in the CAES with the constant-pressure tank, a nonlinear cam transformation mechanism was used by Wang et al. [22]. Their results showed that the working pressure of the system has a significant effect on the energy-saving performance, and with the increase of the working pressure, the amount of energy-saving decreases. Based on literature, storage and discharging pressures are two of the most important parameters affecting the thermodynamic and economic performance of CAES systems. Providing high storage pressure is linked with a set of considerable limitations. In this regard, in order to achieve higher pressures and solve existing limitations, the simultaneous use of CAES and PHES concepts can be considered an attractive solution.

The performance of the proposed systems can be examined in various aspects such as energy, exergy, economics and economics. But examining the system's performance alone is not important and the optimal system's operational conditions needs to always be determined. Various studies have been conducted to optimize the multi -purpose CAES system. Alirahmi et al. [23] proposed a CAES system equipped with hydrogen electrolyzer and optimized the system performance with artificial neural network. They compared four different optimization algorithms and concluded that the PESA-II algorithm was the most ideal for the simultaneous optimization of exergy return efficiency and product cost rate, as objective functions. Alirahmi et al. [24] proposed a CAES system equipped with concentrated solar power and multi-effect desalination and optimized the performance of the system. Their optimization results show that the charge and discharge pressure ratio is one of the most important parameters and by reducing it, the economic and thermodynamic performance of the system improves. They also showed that the use of artificial neural networks can have a significant effect on increasing optimization accuracy and reducing run time. Yin and Sardari [25] proposed a CAES system based on geothermal and solar power plants. They optimized and compared four different scenarios of the proposed system using the MOPSO algorithm. Hai et al. [26] proposed a multi-generation system based on a biomass gasifier-fired steam Rankine cycle (SRC) and CAES system. They optimized the performance of the system in terms of thermodynamics and economy by using ANN and NSGA-II algorithm and showed that the discharge pressure in CAES systems is of great importance and the smaller the charge and discharge pressure difference, the more the system performance will be improved.

As it was mentioned, using constant pressure tanks instead of constant volume tanks eliminates the exergy destruction caused by the regulator valve, increases the production capacity of the system for better peak shaving, reduces the storage tank's volume and increases the energy storage density. According to the studies, considering the advantages of constant pressure tanks and in order to increase the pressure and energy storage capacity, a new method based on PHES and CAES concepts has been suggested. The referenced constant pressure CAES (CP-CAES) system does not have the limitations of the previously proposed systems that are accompanied by high investment costs to obtain high pressure levels. Also, the proposed system can be used alongside all water sources or artificial ponds. On the other hand, in this system, to enhance the functionality and increase the power production of the system, the high temperature energy storage (HTES) unit is used to raise air's temperature fed to the air turbine (AT). The HTES unit replaces the combustion chamber and eliminates creation and release of greenhouse gases to the environment and improves the compatibility of the referenced CP-CAES system with the environment. The heat generated during the air compression process upon discharge results in an increase in the temperature of the discharged air as it is released into the environment. As a result, the system requires a waste heat recovery (WHR) unit to recover the heat produced by the compression processes. On the other hand, the startup time of CAES and WHR systems are not the same, and this will reduce the ultimate functionality of the system in real conditions. In the referenced CP-CAES system, the entire heat of compression is independently recovered by a WHR unit, which consists of an organic Rankine cycle (ORC) equipped with thermoelectric generation (TEG), reheater and internal heat exchanger (IHX). In addition to the environmental benefits, the application of peak shaving, peak shifting, black start, lowering thermal pollution and removing the demand for combusting fossil fuels are the other benefits of the referenced CP-CAES system. In addition to the concerns related to environment mentioned above, an environmentally friendly working fluid which occurs naturally in nature and does not cause ozone depletion and global warming, is utilized in the WHR system, and makes the referenced hybrid system turns into an idea that is entirely ecologically friendly. To investigate the system's functionality thoroughly and precisely, it is examined from energy, exergy, economic and exergoeconomic perspectives. Also, by using artificial neural network (ANN) and genetic algorithm optimization method, the best working conditions are achieved and explained. In addition, Grassmann plots of exergy and cost rates are examined to provide a detailed view into the system's functionality under optimal conditions. At the end, the impact of optimization decision factors on the functionality of the referenced CP-CAES system is investigated. The primary goals of the article are as follows:

- Proposing an innovative compressed air storage system that integrates the principles of CAES and PHES. This system offers several advantages, including increased storage pressure, optimized utilization of the exergy of stored compressed air by eliminating the need for a regulator valve, and enhanced overall production capacity. Moreover, complete discharge of stored compressed air leads to a reduction in storage tank volume and an increase in energy storage density.
- Implementing a HTES unit to supply the necessary energy for elevating the temperature of the compressed air entering the AT, thereby improving the system's overall production capacity and preventing the need for a continuous combustion chamber using fossil fuels.
- Employing a WHR unit, comprising an ORC with reheater, IHX, and TEG, independently to recover waste heat. This not only assists in regulating the system's discharge start time but also enhances its functionality.
- Conducting 4E (energy, exergy, economic and exergoeconomic) analysis to provide a detailed view of the functionality of the referenced system, which is a knowledge gap in body of the science.
- Utilizing genetic algorithm and ANN to accurately perform a multi-criteria optimization to obtain the optimal working conditions while taking into account the economic and thermodynamic factors simultaneously.
- Evaluating the system's feasibility through an in-depth case study that factors in real-world economic conditions and California's hourly electricity pricing.
- Comparing the performance of the proposed system with that of a tank with constant volume and pressure.

2. System description

A representation of the referenced CP-CAES system is shown in Fig. 1. The system's ultimate performance is a combination of the concept of CAES and PHES systems. In the referenced CP-CAES system, compression of air is done in multi phases and then the high-pressure air is stored in storage tanks. The use of constant pressure tanks makes the charging and discharging pressures to be equal and results in considerable growth in the system's capacity for energy production. In this regard, to keep the pressure constant at higher pressures, the concept of PHES can be used, and a pump unit can be utilized to supply high pressures. Also, there is always some waste heat in energy storage systems, which causes heat pollution in the environment. The use of this heat for preheating the compressed air in the discharge process causes the structural complexity of the system. Also, it is not possible to completely recover the wasted heat as the start-up time of different units is not the same. Therefore, the waste energy in the system, such as heat produced by compressing air, is completely transferred to a WHR unit. To achieve a more comprehensive view of the referenced CP-CAES system's functionality, its operation during the two processes of the storage unit and the WHR unit is explained.

2.1. Energy storage unit

Electric energy produced from renewable resources cannot be used in the grid as they have fluctuation. Therefore, low-quality renewable electrical energy and cheap electrical energy from the grid are used to generate heat in the HTES unit and also run the AC train. The ambient air is compressed in three steps by the AC train (states 1–6). Air compression in ACs is accompanied by heat production, which results in increasing the electricity consumption of the ACs. The excess heat generated from the ACs is recovered by using the coolers (C_{1-3}) with synthetic oil (Therminol-VP1). As a result, the power consumed by the ACs is reduced, and the recovered energy is stored with oil in the hot oil tank (HOT). After leaving the last stage of cooling (C_3), air is cooled down to the ambient temperature by passing through the heating heat exchanger (HHX). This reduction in temperature causes that, firstly, the specific volume of compressed air entering the storage tank is decreased and resulting in reducing the size of the storage tank. Second, the energy recovered from the air can be used for district heating. When the compressed air enters the compressed air vessel (CAV) tank, water is discharged from the tank with a volume flow rate and a pressure equivalent to the volume flow rate and pressure of the incoming air to the tank. Considering that the outlet water from the tank has a high pressure (state 20), by passing through a hydraulic turbine (HT), it expands to the ambient pressure and generates power which supplies a part of the system's electricity consumption. In the discharge process, the water is pumped into the tank by the water pump (WP) at a pressure equivalent to the charging pressure, causing the compressed air to be discharged from the tank at a constant pressure. The air's temperature leaving the tank is gone up by passing through a Recuperator (Rec) and $HTES_1$ prior to entering the AT_1. High-pressure and temperature air enters the first stage of ATs. The air expansion process has two stages of heating by HTES, which results in improving the performance of the system and enhancing its production capacity. The air exiting from the last stage of the ATs has a high temperature and its discharge into the air causes thermal pollution (State 16). Therefore, it can be used to preheat the air which results in preventing thermal waste, and heat pollution to the environment and also reducing the electrical power needed in $HTES_1$. And at the end, the air with a lower temperature leaves the Rec and enters the atmosphere.

2.2. Waste heat recovery subsystem

For recovering the waste energy of the referenced CP-CAES system, an ORC cycle equipped with superheater (SH), IHX and TEG is used. The

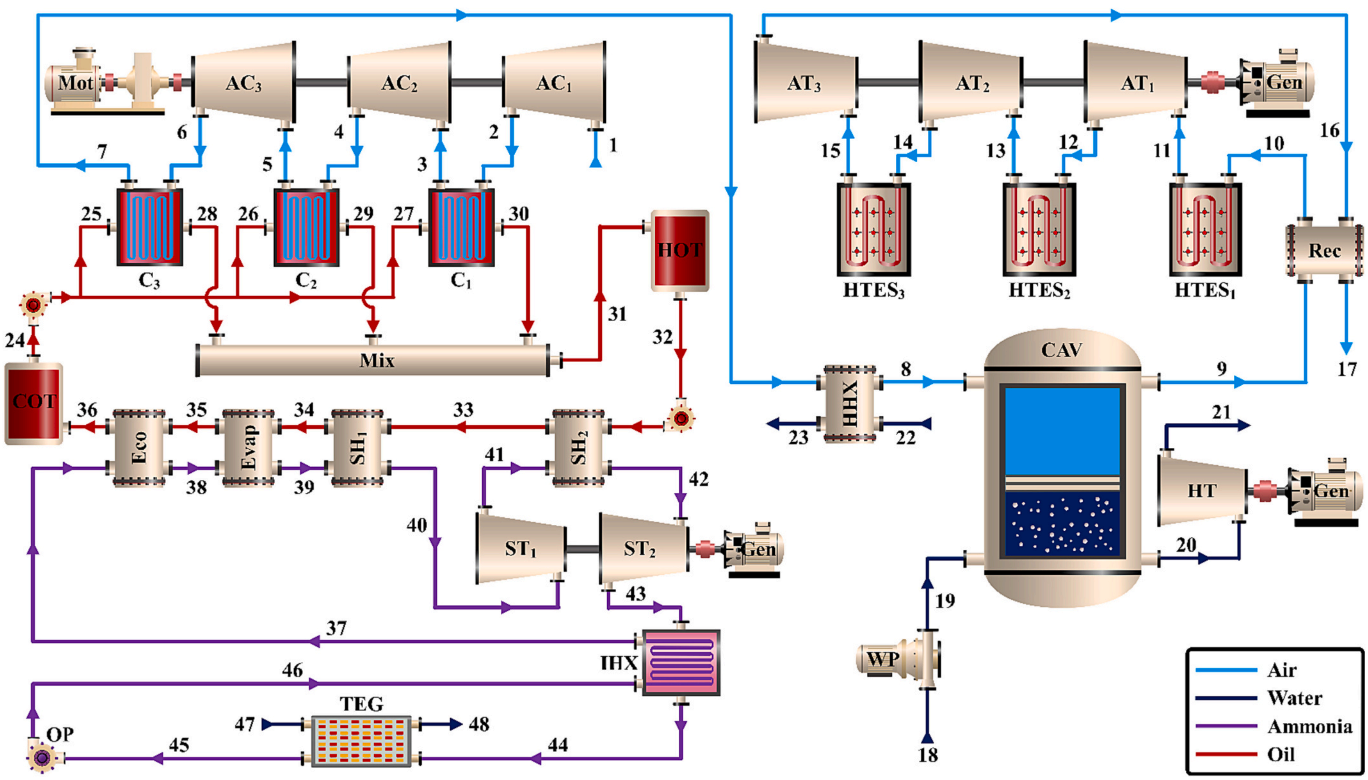

Fig. 1. Diagram of the referenced CP-CAES system.

working fluid used in ORC is ammonia, which is environmentally friendly and does not destroy the ozone layer. Ammonia goes into the orc pump (OP) as a saturated liquid (state 45) and is preheated in the IHX before entering the economizer (Eco). Preheating improves the performance of the whole WHR cycle. After going through another preheating process in the Eco, ammonia enters the evaporator (Evap) as a saturated liquid and leaves it as a saturated vapor. Then, passing through SH_1, it enters the first stage of the steam turbine (ST) in the form of superheat with high pressure and temperature. The working fluid undergoes another heating process in SH_2 before entering the second expansion stage. The outflow from the ST_2 has a high temperature and energy that can be recovered using the IHX (state 43). Finally, ammonia enters the condenser, which is equipped with a TEG. The temperature differential between the condenser's cold and hot flows leads to electricity generation and enhances the cycle performance.

3. System modeling and assessment

For investigating the functionality of the referenced system, energy, exergy, economic, and finally exergoeconomic analysis has been explored.

3.1. Modeling assumptions

For doing the simulation of the referenced system, the below assumptions are made [23,27–29]:

(1) Air is considered to behave like an ideal gas.
(2) Pressure drops, kinetic, and potential energies are disregarded.
(3) The outflow of working fluid from the TEG and Eco is considered to be saturated liquid.

Table 1
Operating conditions of the referenced CP-CAES system.

Parameter	Value	Unit	Reference
Air gas constant	0.287	kJ/kg.K	[10]
Ambient pressure	1.01	bar	[10]
Ambient temperature	300	K	[10]
Charging mass flowrate of CAES	6	kg/s	–
Condenser cooling water temperature	300	K	[30]
Condenser pinch-point temperature difference	5	K	[30]
Efficiency of HTES	90	%	[10]
Heat exchanger pinch-point temperature difference	10	K	[10]
Isentropic efficiency of AT	95	%	[31]
Isentropic efficiency of AC	90	%	[32]
Isentropic efficiency of HT	85	%	[33]
Isentropic efficiency of OP	80	%	[34]
Isentropic efficiency of ST	87	%	[34]
Isentropic efficiency of WP	90	%	[33]
Maximum temperature of HTES	1600	K	[10]
Specific heat capacity of HTES	0.88	kJ/kg.K	[10]
The density of HTES	2100	kg/m^3	[30]

(4) The state of the outflow from the evaporator is considered as saturated vapor.
(5) The pressure of oil tanks (OT) is considered to be equivalent to atmospheric pressure and there is no heat loss in them, as they are perfectly insulated.
(6) The system is examined in steady-state conditions.
(7) All mechanical equipment is thought to have a constant isentropic efficiency.

Table 1 shows the initial values and operating conditions needed to represent the referenced CP-CAES system.

3.2. Mathematical modeling

The energy, mass, economic, and exergoeconomic balance equations are utilized to analyze both the individual components of the system in addition to the entire system to carry out the 4E analysis for the referenced system. The next section contains the equations that are utilized to model the system.

3.2.1. Energy analysis

In steady-state conditions, for a control volume, the equations of mass and energy balance are explained as follow [35]:

$$\sum \dot{m}_{in} = \sum \dot{m}_{out} \tag{1}$$

$$\sum (\dot{m}\cdot h)_{out} - \sum (\dot{m}\cdot h)_{in} = \dot{Q}_{in} - \dot{W}_{out} \tag{2}$$

3.2.2. Exergy analysis

Exergy analysis is one of the vital examinations that should be considered to have a correct simulation [36]. Exergy is the maximum useful work possible during a process [37]. Irreversibility is one of the loss sources in the system. Understanding the number of losses in each process is necessary for improving the system performance which can be achieved with exergy examination [38]. From four elements of exergy, physical, chemical, potential, and kinetic, it is physical exergy that is investigated in this study, as the changes in velocity and height is negligible. The equation for exergy balance is as follows [39]:

$$\dot{E}x_Q + \sum (\dot{m}\cdot ex_{ph})_{in} = \sum (\dot{m}\cdot ex_{ph})_{out} + \dot{E}x_W + \dot{E}x_d \tag{3}$$

where, $\dot{E}x_d$ represent the exergy destruction rate in the process. The remaining parts of the mentioned equation are as [39]:

$$\dot{E}x_W = \dot{W} \tag{4}$$

$$\dot{E}x_Q = \left(1 - \frac{T_0}{T_i}\right) \tag{5}$$

where, $\dot{E}x_W$ and $\dot{E}x_Q$ are rates of exergy for heat transfer and power on the control volume, correspondingly. T_0 and T_i are the absolute temperature in the stream and reference state, respectively. The term ex_{ph} is described as below [40]:

$$ex_{ph} = (h_i - h_0) - (T_0\cdot(s_i - s_0)) \tag{6}$$

The balance equations of exergy and energy rates related to different components are listed in Table 2.

In the referenced CP-CAES system, for waste heat recovery from the ORC subsystem, one TEG device is utilized. The energy balance equation related to the TEG device is given in Table 2; In this regard, we have [43]:

$$\eta_{TEG} = \eta_{Carnot}\frac{\sqrt{1+ZT_m} - 1}{\sqrt{1+ZT_m} + \frac{T_C}{T_H}} \tag{7}$$

here, ZT_m stands for dimensionless figure of merit, that is a key factor in analyzing the TEG. The aforementioned parameter can be gained with using the below equations [43].

$$\eta_{Carnot} = 1 - \frac{T_C}{T_H} \tag{8}$$

$$T_H = \left(\frac{T_{44} + T_{45}}{2}\right) \tag{9}$$

$$T_C = \left(\frac{T_{47} + T_{48}}{2}\right) \tag{10}$$

where T_H and T_C show the hot and cold temperatures of TEG, accordingly. ZT_m which depends on the p and n-type materials utilized in the TEG device, can be obtained by [44]:

$$ZT_m = \frac{(\alpha_p - \alpha_n)^2\cdot T_m}{\left[\sqrt{\sigma_p\cdot k_p} + \sqrt{\sigma_n\cdot k_n}\right]^2} \tag{11}$$

$$T_m = \left(\frac{T_H + T_C}{2}\right) \tag{12}$$

T_m refers to the average temperature of the flow passing across the TEG. σ, k, and α stand for the electrical resistivity, ultimate thermal conductivity and Seebeck coefficient of the p and n-type materials in the TEG, correspondingly.

3.2.3. Economic analysis

The profitability of an energy storage system is highly influenced by the cost of purchasing and selling electricity. So, to have a better economic examination a research case is considered in California, USA. Table 3 represents the mean electricity prices at various times in this state.

It is essential to explore the economic factors associated with grid-scale storage systems in addition to evaluating the system's overall functionality. To achieve this, all the costs and the profits of the system need to be obtained. In order to determine the cost of the installation of CP-CAES, the cost functions for each component are listed in Table 4. For the referenced CP-CAES system the yearly maintenance cost is assumed to be 6 % of the ultimate investment cost [46].

The net present value (NPV) approach is employed to calculate the economic performance of the referenced CP-CEAS system while accounting for all costs. With this approach, the future year's income is adjusted to its current value, considering the rate of interest [56]:

$$NPV = \sum_{y=0}^{L} \frac{ATP_y}{(1+i)^y} - TIC \tag{13}$$

where, L, y, and i stand for the life span of the system, under evaluation year and the rate of interest, respectively. ATP_y is the difference between inflows, TIC is total investment cost and outflows at the conclusion of the Nth year; inflows often come from grants from the government, trade profit, and asset recovery. Additionally, the mainstream comprises of investments, operating capital outflows, taxes, and working expenses. In the referenced CP-CAES system, the system life span and the rate of interest are assumed to be 30 years and 10 %, correspondingly [46]. The payback period indicates the time required for a project to recover its initial investment. In contrast, the dynamic payback period gives considerable attention to considering the time value, a calculation achievable when the cumulative NPV gets zero value. Dynamic payback period equation can be written as: [17]:

$$DPP = |DPP - 1| + \frac{\left|NPV_{|DPP-1|}\right|}{ATP_{|DPP|}} \tag{14}$$

where, $|DPP - 1|$ shows the last year when NPV has zero value, $ATP_{|DPP|}$ indicates the cash flow in the year $|DPP|$, and $\left|NPV_{|DPP-1|}\right|$ represents the

Table 2
Energy and exergy rate balance equations for the referenced CP-CAES system [41,42].

Component	Energy rate and balance equations	Exergy rate and balance equations
AC_1	$\dot{W}_{AC_1} = \dot{m}_1\cdot(h_2 - h_1)$ $\eta_{AC_1} = \frac{h_{2s} - h_1}{h_2 - h_1}$	$Ex_d^{AC_1} = t_{ch}\cdot\left(\dot{E}x_1 - \dot{E}x_2 + \dot{W}_{AC_1}\right)$
AC_2	$\dot{W}_{AC_2} = \dot{m}_3\cdot(h_4 - h_3)$ $\eta_{AC_2} = \frac{h_{4s} - h_3}{h_4 - h_3}$	$Ex_d^{AC_2} = t_{ch}\cdot\left(\dot{E}x_3 - \dot{E}x_4 + \dot{W}_{AC_2}\right)$
AC_3	$\dot{W}_{AC_3} = \dot{m}_5\cdot(h_6 - h_5)$ $\eta_{AC_3} = \frac{h_{6s} - h_5}{h_6 - h_5}$	$Ex_d^{AC_3} = t_{ch}\cdot\left(\dot{E}x_5 - \dot{E}x_6 + \dot{W}_{AC_3}\right)$
AT_1	$\dot{W}_{AT_1} = \dot{m}_{11}\cdot(h_{11} - h_{12})$ $\eta_{AT_1} = \frac{h_{11} - h_{12}}{h_{11} - h_{12s}}$	$Ex_d^{AT_1} = t_{dch}\cdot\left(\dot{E}x_{11} - \dot{E}x_{12} - \dot{W}_{AT_1}\right)$
AT_2	$\dot{W}_{AT_2} = \dot{m}_{13}\cdot(h_{13} - h_{14})$ $\eta_{AT_2} = \frac{h_{13} - h_{14}}{h_{13} - h_{14s}}$	$Ex_d^{AT_2} = t_{dch}\cdot\left(\dot{E}x_{13} - \dot{E}x_{14} - \dot{W}_{AT_2}\right)$
AT_3	$\dot{W}_{AT_3} = \dot{m}_{15}\cdot(h_{15} - h_{16})$ $\eta_{AT_3} = \frac{h_{15} - h_{16}}{h_{15} - h_{16s}}$	$Ex_d^{AT_3} = t_{dch}\cdot\left(\dot{E}x_{15} - \dot{E}x_{16} - \dot{W}_{AT_3}\right)$
COT	$V_{COT} = \frac{3600\cdot\dot{m}_{24}\cdot t_{ch}}{\rho_{24}}$	$Ex_d^{COT} = t_{dch}\cdot\dot{E}x_{36} - t_{ch}\cdot\dot{E}x_{24}$
CAV	$V_{CAV} = \frac{3600\cdot\dot{m}_{18}\cdot t_{ch}}{\rho_{18}} = \frac{3600\cdot\dot{m}_9\cdot t_{dch}}{\rho_9}$	$Ex_d^{CAV} = t_{ch}\cdot\dot{E}x_8 - t_{dch}\cdot\dot{E}x_9$
C_1	$\dot{Q}_{C_1} = \dot{m}_2\cdot(h_2 - h_3) = \dot{m}_{27}\cdot(h_{30} - h_{27})$	$Ex_d^{C_1} = t_{ch}\cdot\left(\dot{E}x_2 + \dot{E}x_{27} - \dot{E}x_3 - \dot{E}x_{30}\right)$
C_2	$\dot{Q}_{C_2} = \dot{m}_4\cdot(h_4 - h_5) = \dot{m}_{26}\cdot(h_{29} - h_{26})$	$Ex_d^{C_2} = t_{ch}\cdot\left(\dot{E}x_4 + \dot{E}x_{26} - \dot{E}x_5 - \dot{E}x_{29}\right)$
C_3	$\dot{Q}_{C_3} = \dot{m}_6\cdot(h_6 - h_7) = \dot{m}_{25}\cdot(h_{28} - h_{25})$	$Ex_d^{C_3} = t_{ch}\cdot\left(\dot{E}x_6 + \dot{E}x_{25} - \dot{E}x_7 - \dot{E}x_{28}\right)$
Eco	$\dot{Q}_{Eco} = \dot{m}_{35}\cdot(h_{35} - h_{36}) = \dot{m}_{37}\cdot(h_{38} - h_{37})$	$Ex_d^{Eco} = t_{dch}\cdot\left(\dot{E}x_{35} + \dot{E}x_{37} - \dot{E}x_{36} - \dot{E}x_{38}\right)$
Evap	$\dot{Q}_{Evap} = \dot{m}_{34}\cdot(h_{34} - h_{35}) = \dot{m}_{38}\cdot(h_{39} - h_{38})$	$Ex_d^{Evap} = t_{dch}\cdot\left(\dot{E}x_{34} + \dot{E}x_{38} - \dot{E}x_{35} - \dot{E}x_{39}\right)$
HHX	$\dot{Q}_{HHX} = \dot{m}_7\cdot(h_7 - h_8) = \dot{m}_{22}\cdot(h_{23} - h_{22})$	$Ex_d^{HHX} = t_{ch}\cdot\left(\dot{E}x_7 + \dot{E}x_{22} - \dot{E}x_8 - \dot{E}x_{23}\right)$
HOT	$V_{HOT} = \frac{3600\cdot\dot{m}_{31}\cdot t_{ch}}{\rho_{31}}$	$Ex_d^{HOT} = t_{ch}\cdot\dot{E}x_{31} - t_{dch}\cdot\dot{E}x_{32}$
$HTES_1$	$\dot{Q}_{HTES_1} = \dot{m}_{10}\cdot(h_{11} - h_{10})$ $\dot{W}_{HTES_1} = \left(\frac{\dot{Q}_{HTES_1}}{\eta_{HTES}}\right)\cdot\left(\frac{t_{dch}}{t_{ch}}\right)$ $M_{HTES_1} = \frac{\dot{Q}_{HTES_1}\cdot t_{dch}}{C_{HTES}\cdot(T_{max_{HTES}} - T_{min_{HTES}})}$	$Ex_d^{HTES_1} = t_{dch}\cdot\left(\dot{E}x_{10} - \dot{E}x_{11}\right) + t_{ch}\cdot\dot{W}_{HTES_1}$
$HTES_2$	$\dot{Q}_{HTES_2} = \dot{m}_{12}\cdot(h_{13} - h_{12})$ $\dot{W}_{HTES_2} = \left(\frac{\dot{Q}_{HTES_2}}{\eta_{HTES}}\right)\cdot\left(\frac{t_{dch}}{t_{ch}}\right)$ $M_{HTES_2} = \frac{\dot{Q}_{HTES_2}\cdot t_{dch}}{C_{HTES}\cdot(T_{max_{HTES}} - T_{min_{HTES}})}$	$Ex_d^{HTES_2} = t_{dch}\cdot\left(\dot{E}x_{12} - \dot{E}x_{13}\right) + t_{ch}\cdot\dot{W}_{HTES_2}$
$HTES_3$	$\dot{Q}_{HTES_3} = \dot{m}_{14}\cdot(h_{15} - h_{14})$ $\dot{W}_{HTES_3} = \left(\frac{\dot{Q}_{HTES_3}}{\eta_{HTES}}\right)\cdot\left(\frac{t_{dch}}{t_{ch}}\right)$ $M_{HTES_3} = \frac{\dot{Q}_{HTES_3}\cdot t_{dch}}{C_{HTES}\cdot(T_{max_{HTES}} - T_{min_{HTES}})}$	$Ex_d^{HTES_3} = t_{dch}\cdot\left(\dot{E}x_{14} - \dot{E}x_{15}\right) + t_{ch}\cdot\dot{W}_{HTES_3}$
HT	$\dot{W}_{HT} = \dot{m}_{20}\cdot(h_{20} - h_{21})$ $\eta_{HT} = \frac{h_{20} - h_{21}}{h_{20} - h_{21s}}$	$Ex_d^{HT} = t_{ch}\cdot\left(\dot{E}x_{20} - \dot{E}x_{21} - \dot{W}_{HT}\right)$
IHX	$\dot{Q}_{IHX} = \dot{m}_{43}\cdot(h_{43} - h_{44}) = \dot{m}_{46}\cdot(h_{37} - h_{46})$	$Ex_d^{IHX} = t_{dch}\cdot\left(\dot{E}x_{43} + \dot{E}x_{46} - \dot{E}x_{44} - \dot{E}x_{37}\right)$
Mix	$\dot{m}_{28}\cdot h_{28} + \dot{m}_{29}\cdot h_{29} + \dot{m}_{30}\cdot h_{30} = \dot{m}_{31}\cdot h_{31}$	$Ex_d^{Mix} = t_{ch}\cdot\left(\dot{E}x_{28} + \dot{E}x_{29} + \dot{E}x_{30}\right) - t_{dch}\cdot\dot{E}x_{31}$
OP	$\dot{W}_{OP} = \dot{m}_{45}\cdot(h_{46} - h_{45})$ $\eta_{OP} = \frac{h_{46s} - h_{45}}{h_{46} - h_{45}}$	$Ex_d^{OP} = t_{dch}\cdot\left(\dot{E}x_{45} - \dot{E}x_{46} + \dot{W}_{OP}\right)$
Rec	$\dot{Q}_{Rec} = \dot{m}_9\cdot(h_{10} - h_9) = \dot{m}_{16}\cdot(h_{16} - h_{17})$	$Ex_d^{Rec} = t_{dch}\cdot\left(\dot{E}x_9 + \dot{E}x_{16} - \dot{E}x_{10} - \dot{E}x_{17}\right)$
ST_1	$\dot{W}_{ST_1} = \dot{m}_{40}\cdot(h_{40} - h_{41})$ $\eta_{ST_1} = \frac{h_{40} - h_{41}}{h_{40} - h_{41s}}$	$Ex_d^{ST_1} = t_{dch}\cdot\left(\dot{E}x_{40} - \dot{E}x_{41} - \dot{W}_{ST_1}\right)$
ST_2	$\dot{W}_{ST_2} = \dot{m}_{42}\cdot(h_{42} - h_{43})$ $\eta_{ST_2} = \frac{h_{42} - h_{43}}{h_{42} - h_{43s}}$	$Ex_d^{ST_2} = t_{dch}\cdot\left(\dot{E}x_{42} - \dot{E}x_{43} - \dot{W}_{ST_2}\right)$
SH_1	$\dot{Q}_{SH_1} = \dot{m}_{33}\cdot(h_{33} - h_{34}) = \dot{m}_{39}\cdot(h_{40} - h_{39})$	$Ex_d^{SH_1} = t_{dch}\cdot\left(\dot{E}x_{33} + \dot{E}x_{39} - \dot{E}x_{34} - \dot{E}x_{40}\right)$
SH_2	$\dot{Q}_{SH_2} = \dot{m}_{32}\cdot(h_{32} - h_{33}) = \dot{m}_{41}\cdot(h_{42} - h_{41})$	$Ex_d^{SH_2} = t_{dch}\cdot\left(\dot{E}x_{32} + \dot{E}x_{41} - \dot{E}x_{33} - \dot{E}x_{42}\right)$

(*continued on next page*)

Table 2 (*continued*)

Component	Energy rate and balance equations	Exergy rate and balance equations
TEG	$\dot{m}_{44}\cdot h_{44}+\dot{m}_{47}\cdot h_{47}=\dot{m}_{45}\cdot h_{45}+\dot{m}_{48}\cdot h_{48}+\dot{W}_{TEG}$ $\eta_{TEG}=\frac{\dot{W}_{TEG}}{\dot{m}_{44}\cdot(h_{44}-h_{45})}$	$Ex_d^{TEG}=t_{dch}\cdot\left(\dot{E}x_{44}+\dot{E}x_{47}-\dot{E}x_{45}-\dot{E}x_{48}+\dot{W}_{TEG}\right)$
WP	$\dot{W}_{WP}=\dot{m}_{18}\cdot(h_{19}-h_{18})$ $\eta_{WP}=\frac{h_{19s}-h_{18}}{h_{19}-h_{18}}$	$Ex_d^{WP}=t_{dch}\cdot\left(\dot{E}x_{18}-\dot{E}x_{19}+\dot{W}_{WP}\right)$

Table 3
Average power costs in the California, USA [45].

System period (hr)	Off-peak times	Purchase cost ($/kWh)	On-peak times	Sales price ($/kWh)
1	03:00–03:59	0.0372	16:00–16:59	0.3087
2	03:00–04:59	0.0387	15:00–16:59	0.2894
3	03:00–05:59	0.0401	15:00–17:59	0.2805
4	02:00–05:59	0.0409	14:00–17:59	0.2644
5	01:00–05:59	0.0420	14:00–18:59	0.2457
6	00:00–05:59	0.0436	13:00–18:59	0.2308
7	00:00–06:59	0.0450	13:00–19:59	0.2188
8	23:00–06:59	0.0464	13:00–20:59	0.2103
9	23:00–07:59	0.0481	13:00–21:59	0.2039
10	23:00–08:59	0.0498	12:00–21:59	0.1964
11	23:00–09:59	0.0508	11:00–21:59	0.1877
12	23:00–10:59	0.0525	11:00–22:59	0.1786
13	22:00–10:59	0.0545	10:00–22:59	0.1703
14	22:00–11:59	0.0578	09:00–22:59	0.1625
15	22:00–12:59	0.0625	08:00–22:59	0.1560
16	21:00–12:59	0.0682	07:00–22:59	0.1501

Table 4
Investment cost formulas for the components of the referenced CP-CAES system.

Component	Investment cost functions	Reference
AC	$Z_{AC}=7900\cdot\dot{W}_{AC}^{0.62}$	[47]
AT	$Z_{AT}=1100\cdot\dot{W}_{AT}^{0.81}$	[47]
CAV	$Z_{CAV}=4042\cdot V_{CAV}^{0.506}$	[48]
C	$Z_C=12000\cdot\left(\frac{A_C}{100}\right)^{0.6}$	[49]
Eco	$Z_{Eco}=130\cdot\left(\frac{A_{Eco}}{0.093}\right)^{0.78}$	[50]
Evap	$Z_{Evap}=130\cdot\left(\frac{A_{Evap}}{0.093}\right)^{0.78}$	[50]
HHX	$Z_{HHX}=12000\cdot\left(\frac{A_{HHX}}{100}\right)^{0.6}$	[49]
HTES	$Z_{HTES}=2.2\cdot M_{HTES}$	[49]
HT	$Z_{HT}=10^{\left(2.2476+1.4965\cdot log_{10}^{W_{HT}}-0.1618\cdot\left(log_{10}^{W_{HT}}\right)^2\right)}$	[51]
IHX	$Z_{IHX}=130\cdot\left(\frac{A_{IHX}}{0.093}\right)^{0.78}$	[50]
Mix	$Z_{Mix}=114.5\cdot\dot{m}_{31}^{0.67}$	[52]
OT (Oil tank)	$Z_{OT}=423\cdot V_{OT}$	[47]
OP	$Z_{OP}=200\cdot\dot{W}_{OP}^{0.65}$	[53]
Rec	$Z_{Rec}=12000\cdot\left(\frac{A_{Rec}}{100}\right)^{0.6}$	[49]
ST	$Z_{ST}=4750\cdot\dot{W}_{ST}^{0.75}$	[53]
SH	$Z_{SH}=130\cdot\left(\frac{A_{SH}}{0.093}\right)^{0.78}$	[50]
Therminol VP-1	$Z_{Oil}=5000\cdot M_{Oil}$	[54]
Cond-TEG	$Z_{TEG}=16000\cdot A_{TEG}^{0.6}+1500\cdot\dot{W}_{TEG}$	[49,55]
WP	$Z_{WP}=10^{\left(3.3892+0.0536\cdot log_{10}^{\dot{W}_{WP}}+0.1538\cdot\left(log_{10}^{\dot{W}_{WP}}\right)^2\right)}$	[51]

absolute value of NPV by year of $|DPP-1|$.

3.2.4. Exergoeconomic analysis

Exergoeconomic analysis is used to calculate the cost of each flow individually based on the exergy rate. Utilizing this method will result in a complete understanding of the cost of fuel in comparison with the price of products for the equipment. As a result, it gives a good framework for enhancing and choosing design elements, resulting in economical outcomes. The following formula can be used to calculate the equipment's cost per hour [57]:

$$\dot{Z}_k=\frac{Z_k.CRF.\varphi}{\tau} \tag{15}$$

where φ and τ stand for the maintenance factor and yearly working hours of the elements, correspondingly. The cost of purchasing each component is shown with Z_k. Additionally, CRF shows the capital recovery factor, and the equation below can be utilized to calculate it [58]:

$$CRF=\frac{i(1+i)^n}{(1+i)^n-1} \tag{16}$$

In equation above i stands for the rate of interest and n shows the life of the system for one year. For converting the estimated cost to the present cost, the equation described below can be used [23]:

$$\text{Current year's cost}=\frac{\text{Initial cost}\times\text{Current year's cost index}}{\text{Cost index of the initial cost's year}} \tag{17}$$

Additionally, the next equation is cost balance equation that is used to determine the component's cost, that aids in determining the stream cost per energy unit and provide a way for calculating the price of fuel and components [59]:

$$\sum\dot{C}_{in,k}+\dot{C}_{Q,k}+\dot{Z}_k=\sum\dot{C}_{out,k}+\dot{C}_{W,k} \tag{18}$$

where;

$$\dot{C}_k=c_k\cdot\dot{E}x_k \tag{19}$$

$$\dot{C}_{W,k}=c_{W,k}\cdot\dot{E}x_{W,k} \tag{20}$$

$$\dot{C}_{Q,k}=c_{Q,k}\cdot\dot{E}x_{Q,k} \tag{21}$$

where, $\dot{C}_{Q,k}$, $\dot{C}_{W,k}$ and c stand for the thermal energy cost, the electricity cost and the cost per unit of exergy, accordingly. The equations describing total cost of products (cp_{Total}) and levelized cost of electricity ($LCOE$) are as follow [60,61]:

$$cp_{Total}=\frac{\dot{Z}_{Total}+\sum_{i=1}^{3}\dot{C}_{W,AT_i}-\dot{C}_{W,HT}}{\sum_{i=1}^{2}\dot{W}_{Out,Total}}\cdot 3.6\cdot 10^{-3} \tag{22}$$

$$LCOE=\frac{TIC+\sum_{y=0}^{L}\frac{(TIC\cdot\varphi+ATC)}{(1+i)^y}}{\sum_{y=0}^{L}\frac{\left(\dot{W}_{Out,total}\cdot t_{dch}\cdot 365\right)}{(1+i)^y}} \tag{23}$$

The auxiliary equations in addition to the cost balance formulas for each element in the system are presented in Table 5.

Table 5
Auxiliary and Cost balance formulas for elements of the referenced CP-CAES system.

Element	Cost balance	Auxiliary equation
AC_1	$\dot{C}_1 + \dot{C}_{W,AC_1} + \dot{Z}_{AC_1} = \dot{C}_2$	$c_{W,AC_1} = c_{Purchase\ of\ electricity}\left(\$/_{GJ}\right); c_1 = 0$
AC_2	$\dot{C}_3 + \dot{C}_{W,AC_2} + \dot{Z}_{AC_2} = \dot{C}_4$	$c_{W,AC_2} = c_{W,AC_1}$
AC_3	$\dot{C}_5 + \dot{C}_{W,AC_3} + \dot{Z}_{AC_3} = \dot{C}_6$	$c_{W,AC_3} = c_{W,AC_1}$
AT_1	$\dot{C}_{11} + \dot{Z}_{AT_1} = \dot{C}_{12} + \dot{C}_{W,AT_1}$	$c_{11} = c_{12}$
AT_2	$\dot{C}_{13} + \dot{Z}_{AT_2} = \dot{C}_{14} + \dot{C}_{W,AT_2}$	$c_{13} = c_{14}$
AT_3	$\dot{C}_{15} + \dot{Z}_{AT_3} = \dot{C}_{16} + \dot{C}_{W,AT_3}$	$c_{15} = c_{16}$
COT	$\dot{C}_{36} + \dot{Z}_{COT} = \dot{C}_{24}$	–
CAV	$\dot{C}_8 + \dot{C}_{19} + \dot{Z}_{CAV} = \dot{C}_9 + \dot{C}_{20}$	$c_{19} = c_{20}$
C_1	$\dot{C}_2 + \dot{C}_{27} + \dot{Z}_{C_1} = \dot{C}_3 + \dot{C}_{30}$	$c_2 = c_3$
C_2	$\dot{C}_4 + \dot{C}_{26} + \dot{Z}_{C_2} = \dot{C}_5 + \dot{C}_{29}$	$c_4 = c_5$
C_3	$\dot{C}_6 + \dot{C}_{25} + \dot{Z}_{C_3} = \dot{C}_7 + \dot{C}_{28}$	$c_6 = c_7$
Eco	$\dot{C}_{35} + \dot{C}_{37} + \dot{Z}_{Eco} = \dot{C}_{36} + \dot{C}_{38}$	$c_{35} = c_{36}$
Evap	$\dot{C}_{34} + \dot{C}_{38} + \dot{Z}_{Evap} = \dot{C}_{35} + \dot{C}_{39}$	$c_{34} = c_{35}$
HHX	$\dot{C}_7 + \dot{C}_{22} + \dot{Z}_{HHX} = \dot{C}_{23} + \dot{C}_8$	$c_7 = c_8; c_1 = 0$
HOT	$\dot{C}_{31} + \dot{Z}_{HOT} = \dot{C}_{32}$	–
$HTES_1$	$\dot{C}_{10} + \dot{C}_{W,HTES_1} + \dot{Z}_{HTES_1} = \dot{C}_{11}$	$c_{W,HTES_1} = c_{W,AC_1}$
$HTES_2$	$\dot{C}_{12} + \dot{C}_{W,HTES_2} + \dot{Z}_{HTES_2} = \dot{C}_{13}$	$c_{W,HTES_2} = c_{W,HTES_1}$
$HTES_3$	$\dot{C}_{14} + \dot{C}_{W,HTES_3} + \dot{Z}_{HTES_3} = \dot{C}_{15}$	$c_{W,HTES_3} = c_{W,HTES_1}$
HT	$\dot{C}_{20} + \dot{Z}_{HT} = \dot{C}_{21} + \dot{C}_{W,HT}$	$c_{20} = c_{21}$
IHX	$\dot{C}_{43} + \dot{C}_{46} + \dot{Z}_{IHX} = \dot{C}_{44} + \dot{C}_{37}$	$c_{43} = c_{44}$
Mix	$\dot{C}_{28} + \dot{C}_{29} + \dot{C}_{30} + \dot{Z}_{Mix} = \dot{C}_{31}$	–
Oil separator	$\dot{C}_{25} + \dot{C}_{26} + \dot{C}_{27} = \dot{C}_{24}$	$c_{25} = c_{26}; c_{25} = c_{27}$
OP	$\dot{C}_{45} + \dot{C}_{W,OP} + \dot{Z}_{OP} = \dot{C}_{46}$	$c_{W,OP} = c_{W,OT_1}$
Rec	$\dot{C}_9 + \dot{C}_{16} + \dot{Z}_{Rec} = \dot{C}_{10} + \dot{C}_{17}$	$c_{16} = c_{17}$
ST_1	$\dot{C}_{40} + \dot{Z}_{ST_1} = \dot{C}_{41} + \dot{C}_{W,ST_1}$	$c_{40} = c_{41}$
ST_2	$\dot{C}_{42} + \dot{Z}_{ST_2} = \dot{C}_{43} + \dot{C}_{W,ST_2}$	$c_{42} = c_{43}$
SH_1	$\dot{C}_{33} + \dot{C}_{39} + \dot{Z}_{SH_1} = \dot{C}_{34} + \dot{C}_{40}$	$c_{33} = c_{34}$
SH_2	$\dot{C}_{32} + \dot{C}_{41} + \dot{Z}_{SH_2} = \dot{C}_{33} + \dot{C}_{42}$	$c_{32} = c_{33}$
TEG	$\dot{C}_{44} + \dot{C}_{47} + \dot{Z}_{TEG} = \dot{C}_{45} + \dot{C}_{48} + \dot{C}_{W,TEG}$	$c_{W,TEG} = c_{W,OT_1}; c_{44} = c_{45}; c_{47} = 0$
WP	$\dot{C}_{18} + \dot{C}_{W,WP} + \dot{Z}_{WP} = \dot{C}_{19}$	$c_{W,WP} = c_{W,AT_1}; c_{18} = 0$

3.3. Performance criteria

The exergy and energy efficiencies can be determined for the waste-heat recovery subsystem since it contributes to electrical power generation. Regarding the first two rules of thermodynamics, the below formulas are used to investigate the performance of the WHR subsystem [30].

$$\eta_{En}^{WHR} = \frac{\dot{W}_{ST_1} + \dot{W}_{ST_2} + \dot{W}_{TEG} - \dot{W}_{OP}}{\dot{m}_{32}\cdot(h_{32} - h_{36})}\cdot 100 \quad (24)$$

$$\eta_{Ex}^{WHR} = \frac{\dot{W}_{ST_1} + \dot{W}_{ST_2} + \dot{W}_{TEG} - \dot{W}_{OP}}{\dot{E}x_{32} - \dot{E}x_{36}}\cdot 100 \quad (25)$$

RTE is employed for the referenced CP-CAES system as there is typically a trade-off between charge and discharge times. There is a component of the discharge period to the charging period in RTE (for energy evaluation) or exergy round trip efficiency (ERTE) (for exergy evaluation), making the RTE or ERTE suitable for determining the functionality of the whole system [62]:

$$RTE = \frac{t_{dch}\cdot\left(\sum_{i=1}^{3}\dot{W}_{AT_i} + \sum_{i=1}^{2}\dot{W}_{ST_i} + \dot{W}_{TEG} - \dot{W}_{OP} - \dot{W}_{WP} + \dot{Q}_{HHX}\right)}{t_{ch}\cdot\left(\sum_{i=1}^{3}\dot{W}_{AC_i} + \sum_{i=1}^{3}\dot{W}_{HTES_i} - \dot{W}_{HT}\right)} \quad (26)$$

$$ERTE = \frac{t_{dch}\cdot\left(\sum_{i=1}^{3}\dot{W}_{AT_i} + \sum_{i=1}^{2}\dot{W}_{ST_i} + \dot{W}_{TEG} - \dot{W}_{OP} - \dot{W}_{WP} + \dot{Q}_{HHX}\cdot\left(1 - \frac{T_{amb}}{T_{23}}\right)\right)}{t_{ch}\cdot\left(\sum_{i=1}^{3}\dot{W}_{AC_i} + \sum_{i=1}^{3}\dot{W}_{HTES_i} - \dot{W}_{HT}\right)} \quad (27)$$

Electrical efficiency (η_{elec}) is among the crucial characteristics of energy storage systems since these systems are used to peak-shift and peak-shave distribution networks. η_{elec} is determined by dividing the system's out power by its power consumption [62].

$$\eta_{elec,\text{stand alone}} = \frac{t_{dch}\cdot\left(\sum_{i=1}^{3}\dot{W}_{AT_i} - \dot{W}_{WP}\right)}{t_{ch}\cdot\left(\sum_{i=1}^{3}\dot{W}_{AC_i} + \sum_{i=1}^{3}\dot{W}_{HTES_i} - \dot{W}_{HT}\right)} \quad (28)$$

Table 6
Verifying the validity of the CAES and ORC subsystems.

System	Parameter	Unit	Simulation	Reference	Error (%)
CAES [64]	P_{Ch}	bar	25.0	25.0	0.00
	P_{Dch}	bar	12.5	12.5	0.00
	T_{HTES}	K	1300	1300	0.00
	t_{Ch}	hr	8.00	8.00	0.00
	t_{Dch}	hr	4.00	4.00	0.00
	$\dot{W}_{AC_1}$	kW	200.9	201.5	0.30
	$\dot{W}_{AC_2}$	kW	201.7	202.4	0.35
	$\dot{W}_{AT}$	kW	1119	1123	0.36
	RTE	%	51.70	51.89	0.37
ORC [65]	$P_{In,OT}$	bar	25.0	25.0	0.00
	$P_{Out,OT}$	bar	0.10	0.10	0.00
	$T_{In,OT}$	K	552.2	552.2	0.00
	$\dot{Q}_{In}$	kW	26.322	26.082	0.92
	$\dot{W}_{OP}$	kW	0.1648	0.1638	0.61
	$\dot{W}_{ST}$	kW	6.6163	6.5456	1.08
	η_{En}	%	24.510	24.431	0.32

$$\eta_{elec} = \frac{t_{dch}\cdot\left(\sum_{i=1}^{3}\dot{W}_{AT_i} + \sum_{i=1}^{2}\dot{W}_{ST_i} + \dot{W}_{TEG} - \dot{W}_{OP} - \dot{W}_{WP}\right)}{t_{ch}\cdot\left(\sum_{i=1}^{3}\dot{W}_{AC_i} + \sum_{i=1}^{3}\dot{W}_{HTES_i} - \dot{W}_{HT}\right)} \quad (29)$$

$$\mathrm{Imp}_{\mathrm{elec}} = \frac{\eta_{elec} - \eta_{elec,\mathrm{stand\ alone}}}{\eta_{elec,\mathrm{stand\ alone}}}\cdot 100 \quad (30)$$

The total storage energy density (TSED) is utilized to determine the ultimate power produced by the system in the discharging period divided by the tank's ultimate volume. TSED is considered as a functionality criterion that is applied to do comparison between the efficiency and volume of the energy storage systems. TSED is explained as follow [63]:

$$TSED = \frac{3.6\cdot\left(\sum_{i=1}^{2}\dot{W}_{GT_i} - \sum_{i=1}^{2}\dot{W}_{CRP_i}\right)\cdot t_{dch}}{V_{LAS} + V_{\mathrm{Propane}}} \quad (31)$$

4. Results and discussions

MATLAB™ and Engineering Equation Solver (EES) computer programs are utilized to do simulations of the referenced CP-CAES system according to the working conditions shown in Table 2 and the equations represented in Section 3. For this purpose, after verifying the validity of the simulated system with using the results of the literature, the optimum working conditions of the referenced CP-CAES system is found via multi-criteria optimization by genetic algorithm. The impact of significant factors on the overall functionality of the system is identified using parametric analysis. Finally, the outcomes of energy, exergy, economic, and exergoeconomic examinations are represented for the optimum working conditions.

4.1. Model validation

The referenced CP-CAES system is a novel energy production system that is examined for the first time in the current study; therefore, each sub-system has been examined and validated with referenced articles. For validation, the design conditions mentioned in the referenced articles are used to model each sub-system. The results of validation are shown in Table 6. Regarding this, the outcomes from the simulated CAES subsystem by Chen et al. [64] and the ORC unit by Sadreddini et al. [65] are compared. As seen in Table 6, due to small variances in all models, the suggested models are valid.

4.2. Multi-criteria optimization

Thermodynamic and economic analysis in addition to parametric study by themselves are not enough to determine sufficient operating mode and selecting the optimum conditions of the referenced CP-CAES system. As a result, multi-criteria optimization with all the key factors acting as decision variables should be applied to obtain the best working condition of the system. The goals of the optimization process are to shorten the payback period and enhance the referenced system's total power output as much as possible. In this regard, an ANN model combined with a genetic algorithm is used.

Table 7
Decision variables and their upper and lower bounds used in optimization.

Parameters	Unit	Lower bound	Upper bound
Charging period	hr	2	16
Discharging period	hr	2	8
Inlet pressure of the ST_1	bar	40	70
Inlet temperature of the ATs	K	950	1450
Pressure of the CAV	bar	40	100
Pressure ratio of the reheat	–	0.55	0.9
Temperature of the HOT	K	450	490

4.2.1. Optimization method

In the current study, for evaluating and optimizing the performance of the system and finding the optimum model, the genetic algorithm is used. As the optimization process is time-consuming, the data obtained from simulations are trained by an ANN model after generating the system's simulation. As a result, the time needed for simulations is decreased considerably from a couple of hours to a couple of minutes. Using the generated model, the energy, exergy, economic, and exergoeconomic evaluations of the referenced CP-CAES system are repeated 3000 times, resulting in generating 3000 random data sets. The objective functions (Payback period, Total output power) are obtained by feeding the generated data to the ANN model. The approach for order of preference by similarity to ideal solution (TOPSIS) deciding factor is applied after optimization to determine the optimum quantity. A schematic representation is displayed in Fig. 2 to give a better view of the objectives of the optimization method. The system's key variables considered as decision-making factors in addition to their minimal and maximal values are represented in Table 7. The decision variables have been chosen from among the various influencing parameters on the system's performance, focusing on those with the most significant impact on its overall efficiency.

4.2.2. Artificial neural network model validation

The coefficient of determination (R^2) is taken into account for accuracy's evaluation of the ANN model. It measures the difference between anticipated outputs with the ground truth results of the simulations. The ideal situation happens when data are placed on Y = X line, meaning that the R^2 is equal to 1. The results shown in Fig. 3 confirm the accuracy and consistency of the trained ANN model as R^2 value for total output power and payback period are 0.99986 and 0.98524, respectively.

4.2.3. Optimization results

As previously noted, multi-criteria optimization is used to obtain the best operational state with considering thermodynamic and economic factors at the same time. For this purpose, the genetic algorithm that is

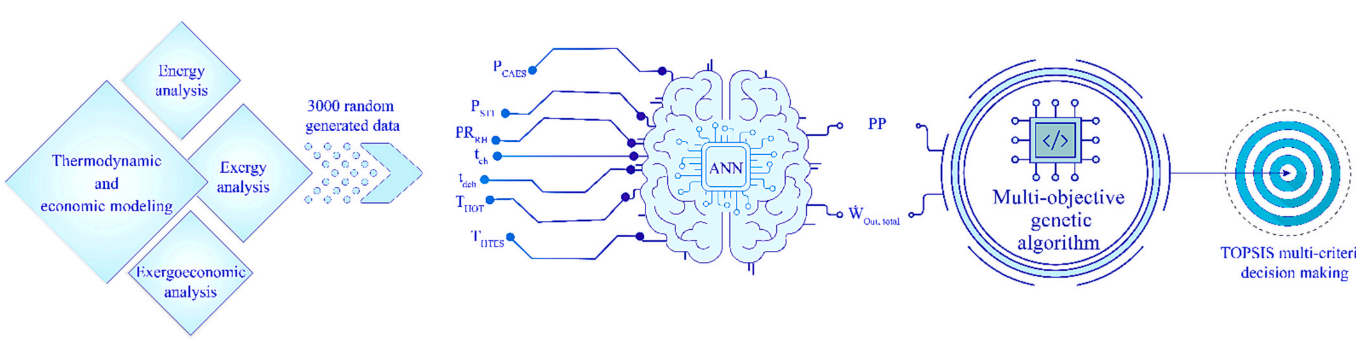

Fig. 2. Multi-objective optimization method.

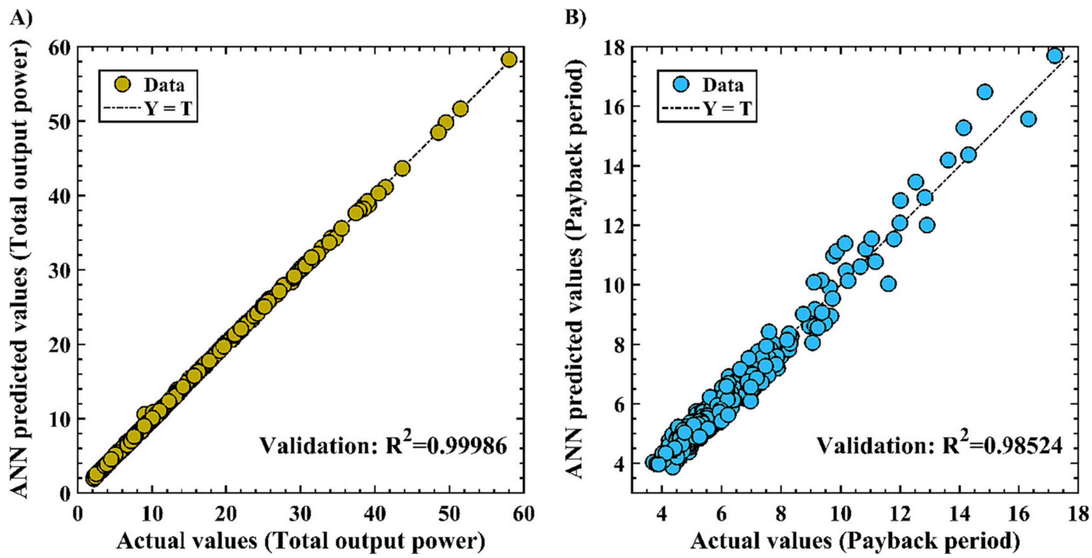

Fig. 3. Artificial neural network validation A) Total output power, B) Payback period.

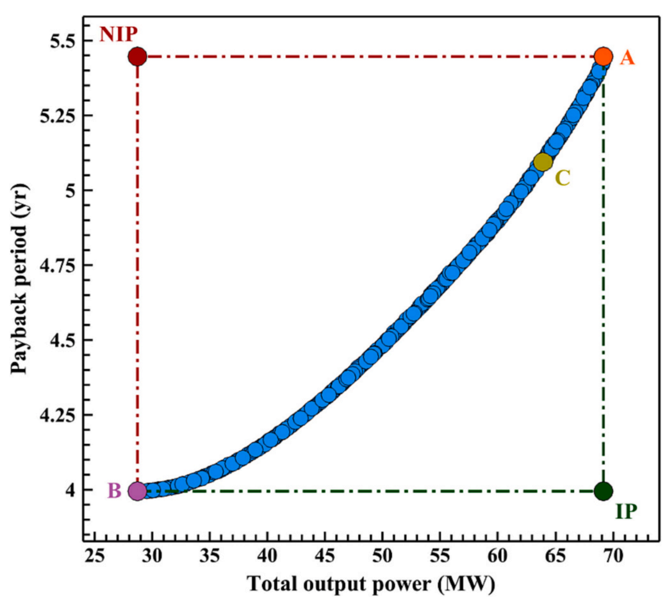

Fig. 4. Pareto frontier of the optimization process.

Table 8
Results of the multi-criteria optimization.

Parameter	Unit	A	B	C
Charging period	hr	15.997	11.527	15.995
Discharging period	hr	2.001	3.125	2.148
Inlet pressure of the ST_1	bar	61.219	42.971	48.602
Inlet temperature of the ATs	K	1396.47	1261.68	1382.89
Pressure of the CAV	bar	99.530	98.277	99.825
Pressure ratio of the reheat	–	0.868	0.899	0.898
Temperature of the HOT	K	489.838	489.970	489.975
Total output power	MW	69.137	28.717	63.927
Payback period	yr	5.447	3.994	5.088

an easy-to-use and robust evolutionary-based algorithm is utilized. The Pareto frontier resulting from the optimization process which is a collection of optimum points, is shown in Fig. 4. Points A and B are ideal points between all existing conditions from a thermodynamic view (highest total output power) and economic view (lowest payback period), respectively. Finally, using the TOPSIS method, the optimal point (C) with trade-off between the payback duration and total output power is selected. Table 8 represents the outcomes obtained from optimization.

Fig. 5 shows the scattered distribution of the decision variables. Each parameter significance in the optimization process is indicated by their distribution between upper and lower bounds. (A, B, D), the values of the pressure of the CAV, the temperature of HOT, and pressure ratio of the reheat at different generations are equivalent to the upper limit as illustrated in Fig. 5 because they have similar impact on both objective functions. That implies, with increasing all the three parameters (restricted to the upper limit) the total power increases and the payback period goes down. While the values of the inlet air temperature to the Ats, the pressure of the inlet fluid to ST_1, the charging and discharging periods (Fig. 5(C, E, F, G)) are distributed within a range. The reason for this behavior is that they have an opposing impact on objective functions and the optimal points need to be selected with considering a trade-off between the economic and thermodynamic performance. As a result, the optimization process is guided by changes in the Inlet pressure of the ST_1, the inlet air's temperature to the ATs and the charging and discharging periods. In the upcoming sections, the impact of decision factors on the functionality of the referenced CP-CAES system is further investigated for the optimal working condition of the system (point C).

5. Results and discussion

The thermodynamic and exergoeconomic properties of the referenced CP-CAES system's currents for the optimal operating conditions are displayed in Table 9. Additionally, Table 10 lists the key outcomes obtained from the energy, exergy, economic, and exergoeconomic analyzes according to the most optimal working condition related to point C in the Pareto frontier, and the governing equations discussed in Section 3. It should also be noted that the results obtained from the network and the EES software are slightly different.

In optimal condition, the referenced CP-CAES system's charging and discharging periods are 16 and 2.15 h, respectively. The AC train takes in fresh air with a mass flow rate of 6 kg/s during the charging periods and compresses it to a pressure of 99.83 bar while consuming power of 3798 kW. The coolers after each compression phase absorb 3393 kW of the excess heat produced by the AC train. The absorbed heat is passed to the oil and oil at 490 K is transferred and kept in the HOT. The compressed air temperature decreases with passing through the cooler

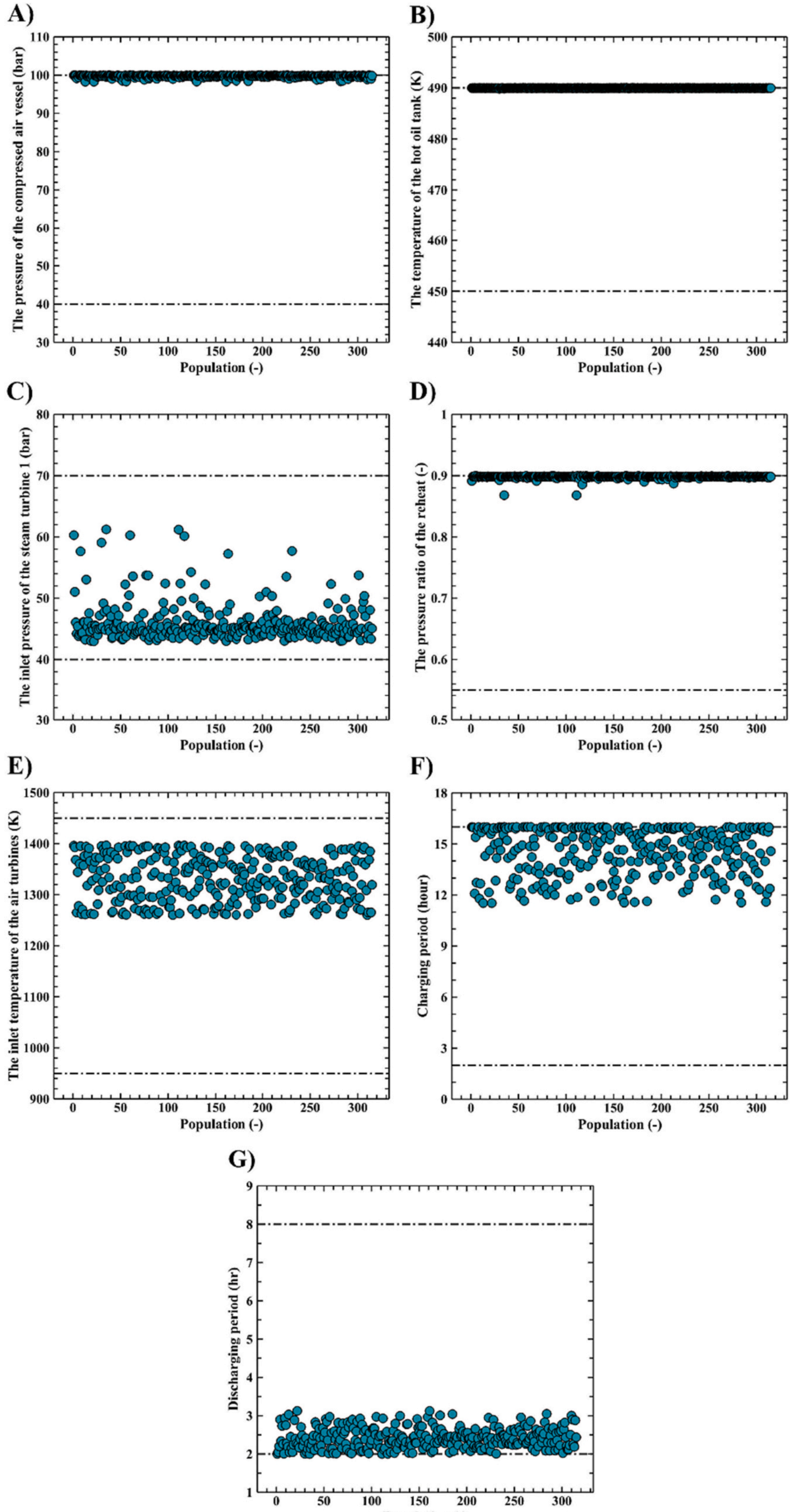

Fig. 5. Decision parameters' dispersed distribution: A) The pressure of the CAV, B) The temperature of the HOT, C) The Inlet pressure of the ST_1, D) The pressure ratio of the reheat, E) The inlet air's temperature to the ATs, F) Charging period, and G) Discharging period.

Table 9
The outcomes of thermodynamic and exergoeconomic analyses for the currents in the referenced CP-CAES.

State	Fluid	$\dot{m}(kg/s)$	$T(K)$	$P(bar)$	$h(kJ/kg)$	$s(kJ/kg{\cdot}K)$	$Ex(MWh)$	$c(\$/GJ)$	$\dot{C}(\$/hr)$
1	Air	6.000	300.0	1.010	300.4	5.703	0.000	0.000	0.000
2	Air	6.000	481.4	4.670	484.2	5.742	16.52	23.38	86.91
3	Air	6.000	367.1	4.670	368.0	5.467	13.28	23.38	69.90
4	Air	6.000	586.0	21.59	592.7	5.506	33.72	23.07	175.1
5	Air	6.000	367.1	21.59	368.0	5.027	25.93	23.07	134.7
6	Air	6.000	586.0	99.83	592.7	5.066	46.37	22.98	239.9
7	Air	6.000	367.1	99.83	368.0	4.588	38.59	22.98	199.6
8	Air	6.000	310.0	99.83	310.5	4.417	37.97	22.98	196.4
9	Air	44.69	300.0	99.83	300.4	4.384	37.96	6.528	415.4
10	Air	44.69	960.6	99.83	1002	5.604	70.13	5.826	684.9
11	Air	44.69	1383	99.83	1495	6.029	105.27	5.312	937.3
12	Air	44.69	970.6	21.59	1013	6.055	58.23	5.312	518.5
13	Air	44.69	1383	21.59	1495	6.468	92.61	4.928	765.1
14	Air	44.69	970.6	4.670	1013	6.495	45.57	4.928	376.5
15	Air	44.69	1383	4.670	1495	6.908	79.96	4.649	623.1
16	Air	44.69	970.6	1.010	1013	6.934	32.92	4.649	256.5
17	Air	44.69	311.3	1.010	311.8	5.740	0.020	4.649	0.110
18	Water	398.7	300.0	1.010	112.6	0.393	0.000	0.000	0.000
19	Water	398.7	300.5	99.83	123.6	0.397	8.470	17.56	249.5
20	Water	53.54	300.0	99.83	121.6	0.390	8.470	17.56	33.49
21	Water	53.54	300.2	1.010	113.2	0.395	0.000	17.56	0.001
22	Water	1.651	300.0	1.010	112.6	0.393	0.000	0.000	0.000
23	Water	1.651	350.0	1.010	321.8	1.038	0.420	35.27	3.293
24	Oil	13.34	357.1	1.010	117.2	0.365	1.740	40.85	11.71
25	Oil	3.929	357.1	1.010	117.2	0.365	0.510	40.85	4.650
26	Oil	3.929	357.1	1.010	117.2	0.365	0.510	40.85	4.660
27	Oil	5.488	357.1	1.010	117.2	0.365	0.710	40.85	6.510
28	Oil	3.929	531.3	1.010	460.3	1.141	7.440	26.93	45.06
29	Oil	3.929	531.3	1.010	460.3	1.141	7.450	27.02	45.20
30	Oil	5.488	426.7	1.010	244.2	0.690	3.320	31.66	23.62
31	Oil	13.34	490.0	1.010	371.4	0.967	17.45	29.03	113.9
32	Oil	99.39	490.0	1.010	371.4	0.967	17.45	4.056	118.6
33	Oil	99.39	486.7	1.010	364.7	0.953	16.87	4.056	114.8
34	Oil	99.39	450.0	1.010	289.9	0.794	11.15	4.056	75.80
35	Oil	99.39	370.7	1.010	140.9	0.430	2.610	4.056	17.73
36	Oil	99.39	357.1	1.010	117.2	0.365	1.740	4.056	11.71
37	R717	18.07	337.5	48.60	513.9	2.005	13.46	10.59	238.9
38	R717	18.07	360.7	48.60	644.0	2.378	14.17	10.58	251.3
39	R717	18.07	360.7	48.60	1464	4.650	19.52	9.851	322.3
40	R717	18.07	476.7	48.60	1875	5.653	23.79	9.247	368.8
41	R717	18.07	466.9	43.65	1855	5.659	22.96	9.247	355.9
42	R717	18.07	480.0	43.65	1892	5.738	23.50	9.196	362.1
43	R717	18.07	397.1	16.37	1725	5.802	16.27	9.196	250.7
44	R717	18.07	356.7	16.37	1618	5.517	15.42	9.196	237.8
45	R717	18.07	315.0	16.37	399.8	1.673	12.89	9.196	198.8
46	R717	18.07	316.3	48.60	406.7	1.678	13.11	10.18	223.9
47	Water	517.6	300.0	1.010	112.6	0.393	0.000	0.000	0.000
48	Water	517.6	310.0	1.010	154.4	0.530	0.760	42.81	54.41

sections and it enters the CAV with a temperature close to the ambient temperature. Lowering the temperature of the entering air to the storage tank causes a considerable impact on reduction of the storage tank's volume. Then, as a result of entering the high-pressure air into the storage tank, the water leaves the tank and produces 450.2 kW of electricity by passing a HT. The generated electricity provides a part of electrical power needed in the HTESs. The rest of required portion of electricity in HTESs is provided by cheap and surplus electricity of the network. After the charging process is complete, 3080 m^3 air with the pressure of 99.83 bar is stored in the CAV which is 52.53 % lower than that for a tank with constant volume (if the ratio of charge-to-discharge pressure of the constant volume tank is 3).

During the discharging process, a WP with 4383 kW power consumption pumps water into the CAV with a pressure of 99.83 bar. Consequently, the stored compressed air in the CAV leaves it with a mass rate of 44.69 kg/s and a pressure equal to the pressure of inlet water to the tank (99.83 bar). The outlet air from CAV goes toward AT train for power generation. To enhance the system's functionality and reduce waste heat, air is preheated by the recuperator (Rec) and then heated to 1383 K by $HTES_1$ before entering the AT_1. Also, to raise the system's capacity for production, the compressed air entering the AT train is reheated during expansion using HTESs. The amount of heat discharged from HTESs into the air is about 65,156.0 kW. As a result of air expansion in the ATs, 64,649.0 kW power is generated for peak shaving. Also, throughout the discharge process, the heat saved in the HOT is recovered by the WHR subsystem which results in production of 3617.0 kW of excess power. According to the thermodynamic analysis RTE, ERTE and η_{Elec} of the referenced system are equal to 68.28 %, 66.01 % and 65.63 %, respectively.

In energy systems, it is crucial to investigate the irreversibility and destructive portion of the transferred energy in the system. Therefore, exergy can be utilized as an alternative to energy to have a better understanding of the thermodynamic processes. Grassmann's detailed diagram is represented in Fig. 6 to give a better view of the energy transfer in the referenced CP-CAES system's streams in addition to the components' exergy destruction. The thickness of each stream shows the quantity of its exergy. The diagram is based on MWh in order to give a more detailed comparison of energy streams as the system has different charging and discharging periods.

During the charging period, air with zero exergy rate enters the AC train and experience compression, with 60.58 MWh power consumption and 3.36 MWh exergy destruction. The excess heat produced by ACs is

Table 10
The Outcomes of energy, exergy, economic, and exergoeconomic analyses for the referenced CP-CAES system.

Parameter	Unit	Value	Parameter	Unit	Value
cp_{Total}	$/GJ	21.15	*RTE*	%	68.28
DPP	yr	5.113	TIC	$M	27.68
ERTE	%	66.01	Total profit	$M	40.02
η_{elec}	%	65.63	*TSED*	MJ/ m^3	81.10
η_{En}^{WHR}	%	14.31	V_{CAV}	m^3	3080
η_{Ex}^{WHR}	%	49.43	V_{COT}	m^3	759.1
Ex_d^{Total}	MWh	70.66	V_{HOT}	m^3	856
LCOE	$/MWh	190.4	$\dot{W}_{AC_1}$	kW	1103
$\dot{Q}_{C_1}$	kW	697	$\dot{W}_{AC_2}$	kW	1348
$\dot{Q}_{C_2}$	kW	1348	$\dot{W}_{AC_3}$	kW	1348
$\dot{Q}_{C_3}$	kW	1348	$\dot{W}_{AT_1}$	kW	21,550
$\dot{Q}_{Eco}$	kW	2351	$\dot{W}_{AT_2}$	kW	21,550
$\dot{Q}_{Evap}$	kW	14,815	$\dot{W}_{AT_3}$	kW	21,550
$\dot{Q}_{HHX}$	kW	345.3	$\dot{W}_{HT}$	kW	450.2
$\dot{Q}_{HTES_1}$	kW	22,056	$\dot{W}_{HTES_1}$	kW	3290
$\dot{Q}_{HTES_2}$	kW	21,550	$\dot{W}_{HTES_2}$	kW	3215
$\dot{Q}_{HTES_3}$	kW	21,550	$\dot{W}_{HTES_3}$	kW	3215
$\dot{Q}_{IHX}$	kW	1937	$\dot{W}_{OP}$	kW	126.1
$\dot{Q}_{Rec}$	kW	31,331	$\dot{W}_{ST_1}$	kW	353.8
$\dot{Q}_{SH_1}$	kW	7428	$\dot{W}_{ST_2}$	kW	3020
$\dot{Q}_{SH_2}$	kW	647.5	$\dot{W}_{TEG}$	kW	369.2
$\dot{Q}_{TEG}$	kW	22,020	$\dot{W}_{WP}$	kW	4383

recovered by coolers and passed to the oil with the ultimate exergy destruction of 2.33 MWh. High-temperature oil with an exergy of 17.45 MWh is stored in the HOT. Compressed air enters the CAV with an exergy rate of 39.97 MWh. It causes water to leave the CAV with an exergy rate of 8.47 MWh, generating 7.20 MWh of electricity by passing a HT with 1.27 exergy destruction. The produced electricity provides a part of the needed electrical power in the HTESs. During discharging, WP increases the exergy rate of the inlet water to the CAV from 0.0 to 8.47 MWh, consuming 9.41 MWh power, and destroying 0.94 MWh exergy. It causes the compressed air leaves the storage tank with an exergy rate of 37.96 MWh. The out air from CAV is preheated in the Rec and experiences a growth of 32.17 MWh in its exergy rate, reaching the largest exergy rate in the system, 70.13 MWh. HTESs consume 155.46 MWh of electrical power from the network to reheat the air and help the ATs to produce a total of 138.84 MWh electrical power with an ultimate 2.28 MWh exergy destruction. Ammonia in the ORC cycle has heat exchange with high-temperature outlet oil from HOT. Its exergy rate increases from 13.46 MWh to 23.79 MWh after passing through the Eco, Evap, and SH_1 before entering the ST_1. The ultimate energy production in STs is equal to 7.25 MWh with total exergy destruction of 0.81 MWh.

According to Fig. 6, of all the components in the referenced CP-CAES system, the exergy destruction of the HTESs is the highest. They totally cause 51.55 MWh destruction in the exergy rate which accounts for more than 70 % of the total exergy destruction in the system. Much of the exergy destruction by the HTESs happens during charging process as the electricity needs to be turned into heat using resistive wires and stored in concrete. The destruction of exergy of the HTESs throughout discharging period happens when the energy saved in concrete is released into the air. The Evap in the ORC cycle has the next highest value of exergy destruction. The exergy destruction of Evap is almost the same as the total exergy destruction of all three ACs with the next rank in exergy destruction. The destruction of exergy in ACs is due to their compression ratio. The lowest exergy destructions of components are related to the ST_1 and the SH_2 in the ORC cycle. Finally, HOT and COT have zero exergy destruction.

The Sankey diagram, Fig. 7, is plotted to better represent exergoeconomic analysis. A good view of the economic performance of the system can be gained by considering the flow rate of streams. During the charging period, AC train consumes cheap and surplus electricity at the cost of 259.04 $/hr to compress air. The outlet water from the CAV generates electricity at the rate of 35.80 $/hr by passing a HT. During the charging period, 662.84 $/hr of electricity is consumed in HTESs provided by cheap electricity of the network, and during the discharging period electricity with a total cost rate of 2706.1 $/hr is generated in three ATs. In the ORC cycle, two STs and TEG generate electricity with cost rates of 457.5 $/hr and 71.47 $/hr, respectively. Regarding the investment costs, three ATs, two STs, and TEG account for the highest values with 1532.1 $/hr, 333.19 $/hr, and 86.91 $/hr (almost equal to that for three HTESs), respectively. Regarding the exergoeconomic evaluation, the total cost of products (cp_{Total}), and levelized cost of the electricity (LCOE) are 21.15 $/GJ and 190.4 $/MWh, respectively.

It is important to know the cost of each component in the system. Each component's cost is mentioned in Table 11. The total cost of the system is equal to $ 27.68 M. Much of the costs are related to the CAES cycle. The highest costs belong to three ATs, three HTESs, and oil with 10.68 (38.6 %), 6.45 (23.3 %), and $ 3.84 M (13.9 %) of the total cost, respectively. The rest of the costs are related to the ORC cycle with 9 components which account for 11.4 % ($ 3.15 M) of the total cost, having two STs as the most expensive components, $ 2.32 M in total. The ORC cycle is employed to enhance the system's functionality. Regarding the fact that using the ORC cycle leads to 6 % improvement in the electrical efficiency of the whole system and its cost is not high compared to the total costs of the system, utilizing the ORC cycle is economical.

The profitability of an energy storage system is highly influenced by the cost of purchasing and selling electricity. So, to have a better economic examination a research case is considered in California, USA. Table 3 represents the mean electricity prices at different daily hours in California. Considering the design conditions represented in Tables 1 and 8, the referenced CP-CAES system charges in 16 h and discharges in 2.15 h. According to the economic analysis's outcomes, the payback is 5.113 years and the ultimate profit generated is equal to $ 40.02 M.

6. Parametric analysis

The functionality of the modeled system is constantly subject to change due to a variety of factors. As a result, it is essential to examine the key parameters which is done in this section.

6.1. The pressure of the CAV

The effect of the pressure of CAV on the functionality of the referenced CP-CAES system is shown in Figs. 8 and 9. There is a dashed line that specifies the charging pressure of the optimal case (point C) equals to 99.83 bar. With increasing the pressure of the CAV, the compression ratio of the ACs goes up which results in increasing the consumption power of them. With increasing the pressure also, the enthalpy of the inlet air to the HTESs increases. Consequently, based on the energy balance equation, the needed power in HTESs goes up. Increasing the consumption power in the HTESs and ACs results in an upward trend of the needed inlet power to the system. Also, raising the pressure of the storage tank results in more power production by the ATs. As higher pressure of the inlet air to the ATs causes expansion ratio of AT goes up. Therefore, with increasing the pressure of CAV, produced power and needed inlet power of the system both increase. The reason of downward trend of RTE, ERTE and η_{Elec} is that the raise in needed input power to the system is higher than that for power generation of the system because of increasing the CAV pressure. By raising the compression ratio of the ACs, the heat production of the AC train goes up which results in more waste heat recovery by the oil in the cooling loop. As the temperature of the HOT is constant, based on the energy balance equation, the mass flow rate of the oil needs to go up to recover more energy produced by the ACs. Considering energy balance equation in the heat exchangers of the ORC cycle, SHs, Eco and Evap, with increasing the oil mass rate in the cooling loop, the mass rate of the working fluid of ORC cycle goes up.

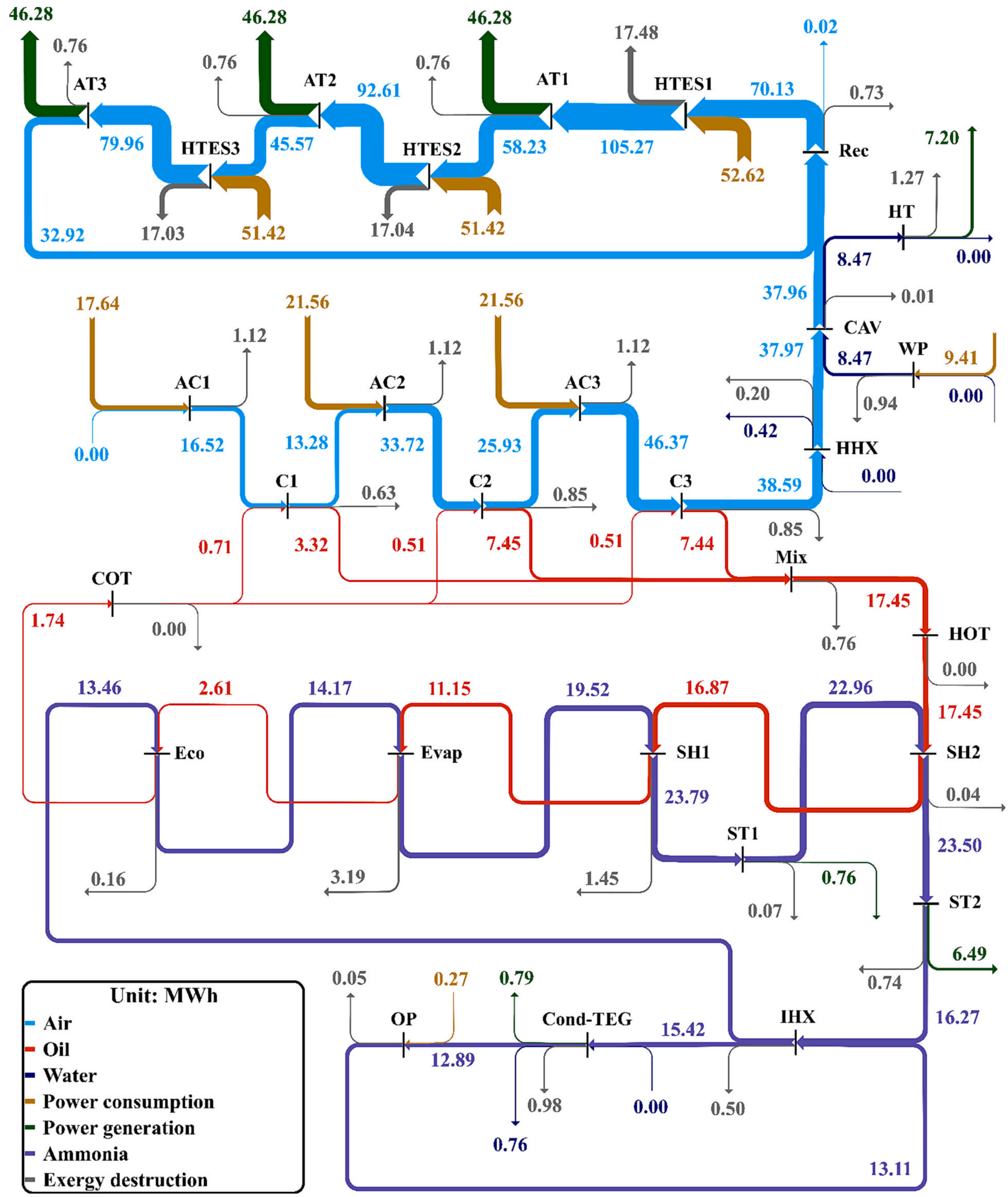

Fig. 6. The Grassmann diagram showing exergy rates in different streams of the referenced CP-CAES system.

The higher mass rate in ORC cycle leads to more power production of the STs and as a result upward trend of Imp_{Elec}. By raising the flow rate in the cooling loop and the ORC cycle, the components in both subsystems need to have bigger sizes. Also, higher mass flow rate in the cooling cycle leads to higher amount of oil. In addition, with increasing the expansion ratio of ATs and enthalpy of inlet air to the HTESs, the capacity and size of these components needs to be larger. All in all, increasing the charging pressure causes a boost in overall cost rate. As it causes the size of some of the components to goes up and the components with bigger size are more expensive. As it was explained earlier, rising the charging pressure leads to increasing the total power generation and as a result more electricity sold by the system. The price of the sold electricity to the network is much higher than the ultimate cost related to input electricity power to the system, maintenance and purchasing the components. Thus, the overall system's profit is growing and consequently the payback is decreasing with increasing the charging pressure.

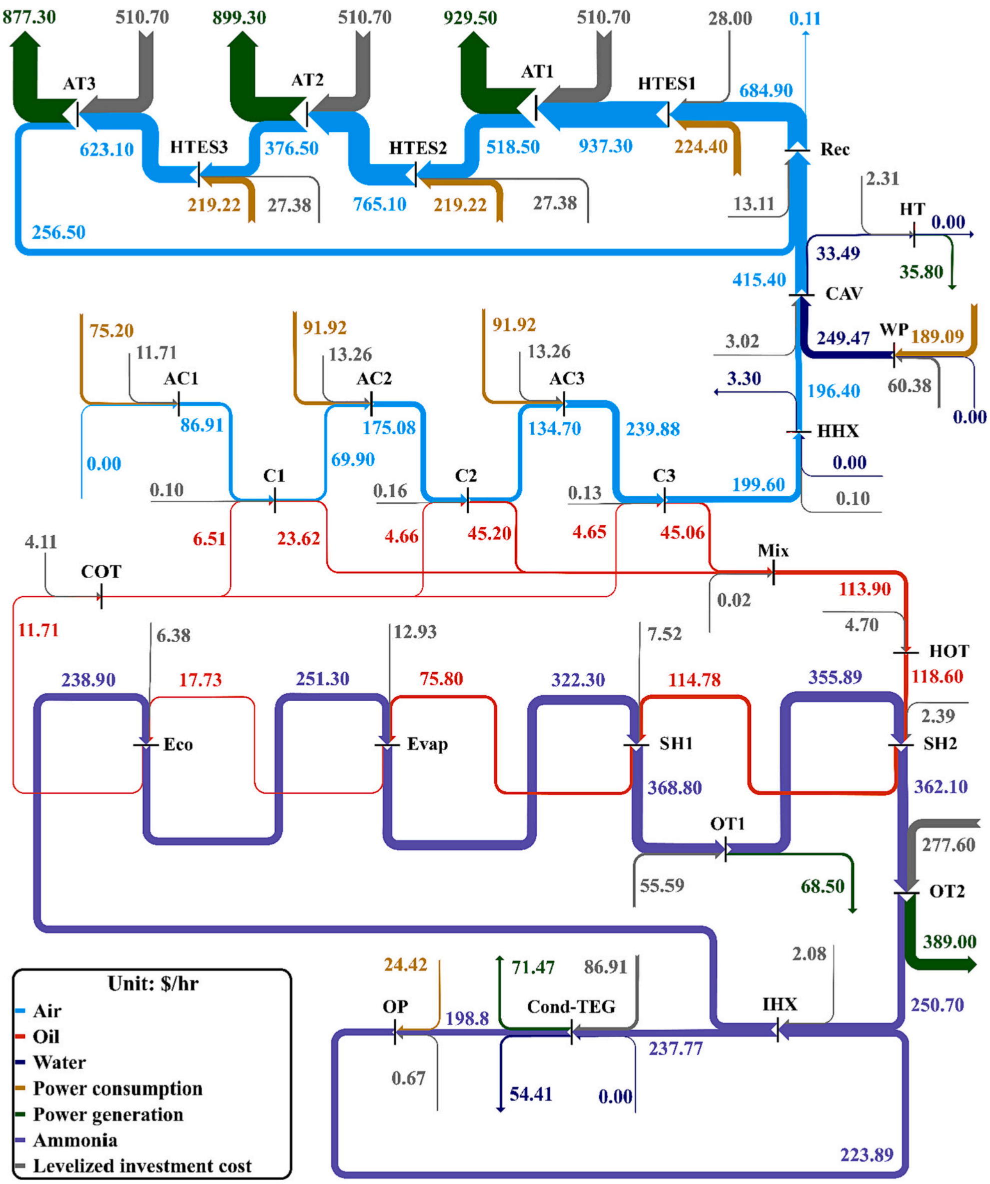

Fig. 7. The Sankey diagram for cost rate of different streams in the referenced CP-CAES system.

Table 11
Investment cost of equipment in the referenced CP-CAES system.

Component	Investment cost ($)	Component	Investment cost ($)
AC_1	608,031	HT	120,022
AC_2	688,636	$HTES_1$	2,182,000
AC_3	688,636	$HTES_2$	2,132,000
AT_1	3,560,000	$HTES_3$	2,132,000
AT_2	3,560,000	IHX	14,499
AT_3	3,560,000	Mix	649.8
C_1	5409	Oil	3,842,000
C_2	8034	OP	4640
C_3	8034	Rec	91,381
CAV	235,385	SH_1	52,691
COT	321,114	SH_2	16,671
Eco	44,396	ST_1	387,484
Evap	90,282	ST_2	1,935,000
HHX	5356	TEG	605,903
HOT	362,095	WP	420,872

6.2. The temperature of the HOT

The impact of the temperature of HOT on the functionality of the referenced CP-CAES system is presented in Figs. 10 and 11. With raising the temperature of the HOT, the produced heat by the ACs and the heat exchanged in the cooler train remains unchanged. As a result, the stored energy in the HOT does not change. Having constant energy rate, according to the energy balance equation, with increasing the temperature of the HOT, oil mass rate needs to be decreased. Therefore, the oil mass rate passing through the coolers as well as HOT goes down. The temperature of the inlet fluid to the STs in ORC cycle is directly dependent on the temperature of HOT as the entering stream to the STs has heat exchange with the out stream from the HOT. Therefore, the temperature and the enthalpy of the inlet fluid to the STs rises with increasing the temperature of HOT. Based on the energy balance equation, reduction in the oil mass rate results in decreasing the mass rate of the working fluid in the ORC cycle as well. Thus, the rate of the fluid in the STs decreases that has a negative impact on the power production of the STs. However, the temperature rise compared to the mass flow reduction of the inlet fluid to the STs shows higher impact on their power production.

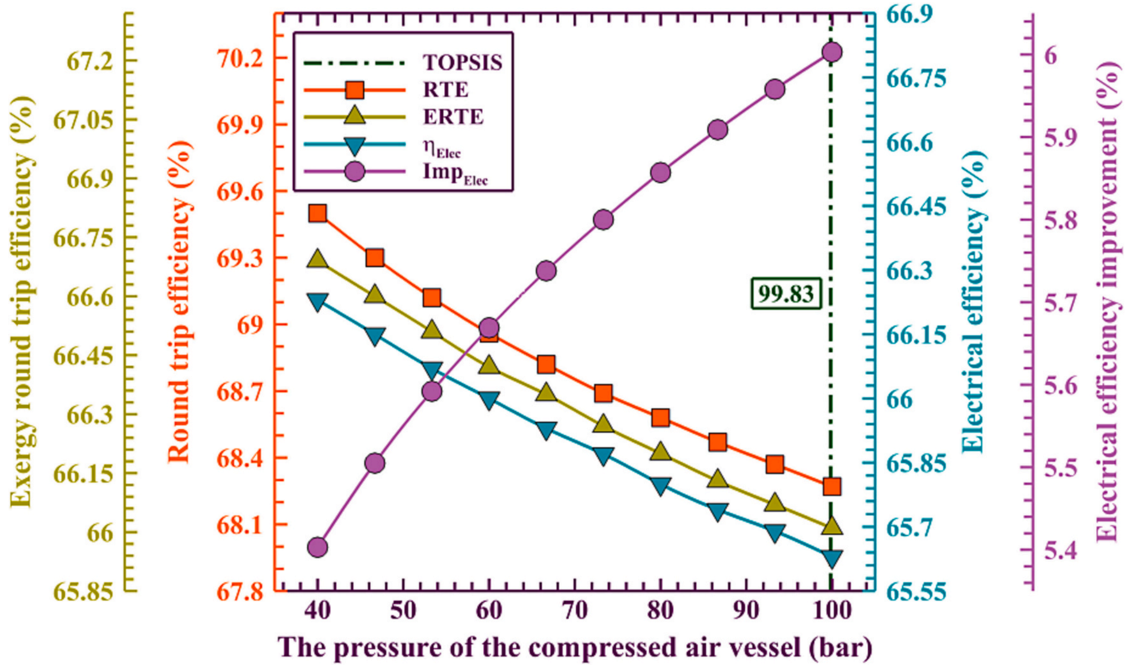

Fig. 8. CAV pressure impact on the RTE, ERTE, η_{Elec} and Imp_{Elec} in the referenced CP-CAES system.

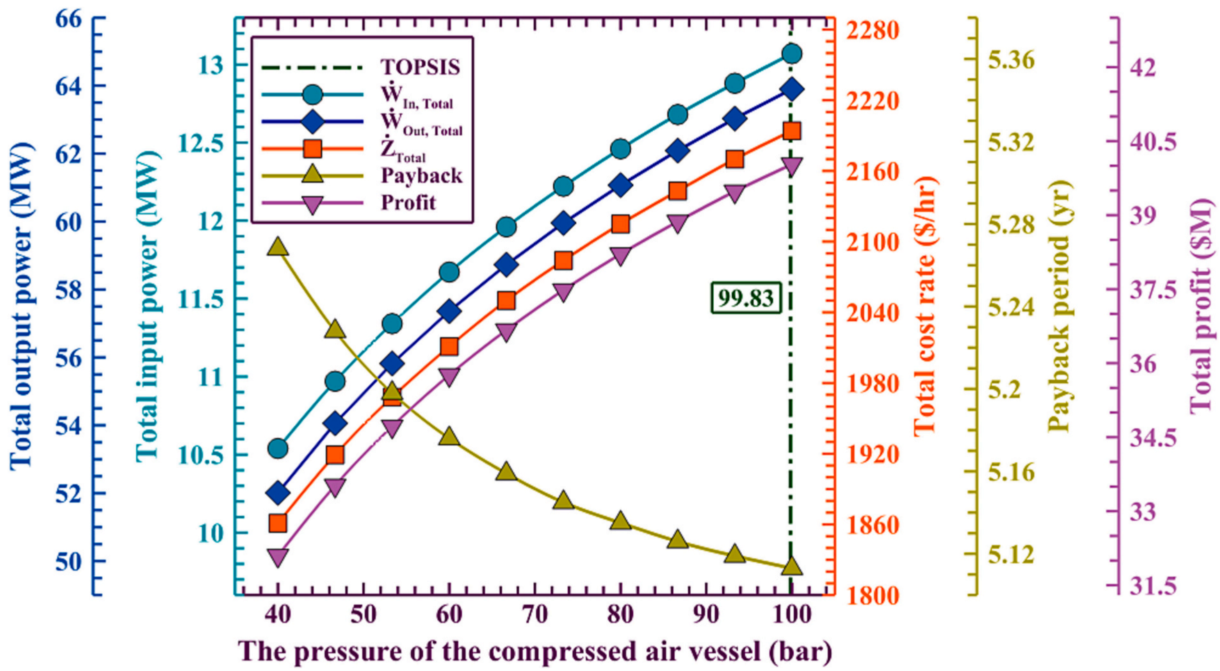

Fig. 9. CAV pressure impact on the total output power, total input power, total cost rate, payback period and total profit in the referenced CP-CAES system.

This leads to a boost in total power production of the ORC cycle which causes RTE, ERTE, and Imp_{Elec} to go up. On the other hand, decreasing the total heat exchanged in the 4 heat exchangers of the ORC cycle, SHs, Eco and the Evap, results in higher efficiency of the ORC cycle. As the total heat exchanged of the ORC cycle has an inverse impact on the ORC cycle's efficiency, based on Eqs. (22) and (23). With increasing the inlet temperature of the STs, their capacity and as a result their cost go up. Reduction in the fluid rate going through the heat exchangers in the ORC cycle causes their size and consequently their price to decrease. With a decrease in the rate of the oil in the cooling cycle the cost of the needed oil also experiences a decrease. Finally, the total cost rate shows an upward trend which is illustrated in Fig. 11. With increasing the out power of the system, the ultimate profit and payback of the whole system experience upward and downward trends, respectively. As the impact of the increase in power out on the profit is higher than the growth in the cost rate. Totally, increasing the temperature of the HOT results in higher efficiency and power out of the ORC cycle and also causes the profit of the system to increase.

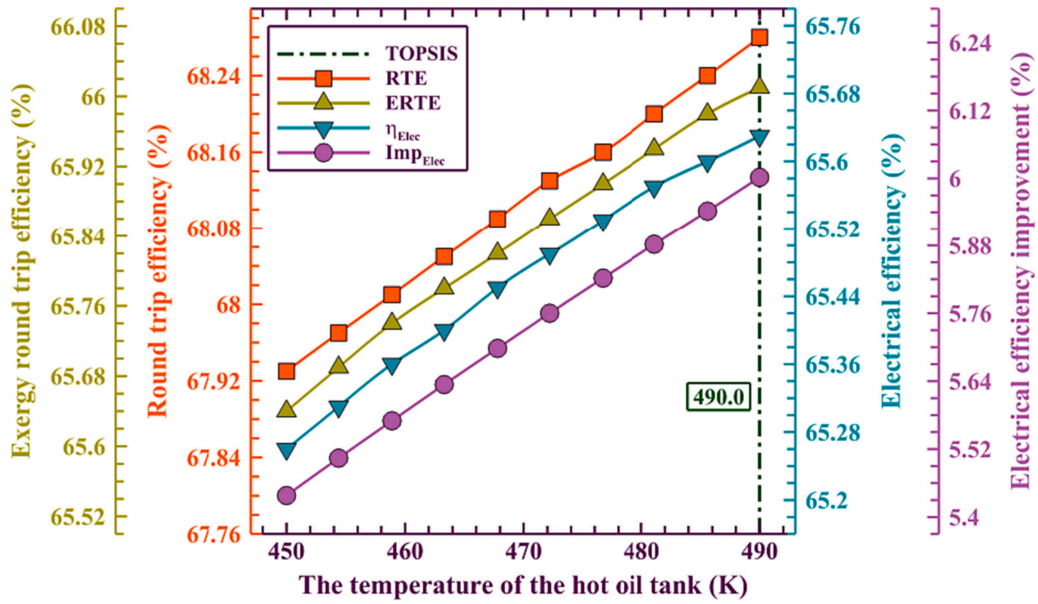

Fig. 10. The impact of the temperature of HOT on the RTE, ERTE, η_{Elec} and Imp_{Elec} in the referenced CP-CAES system.

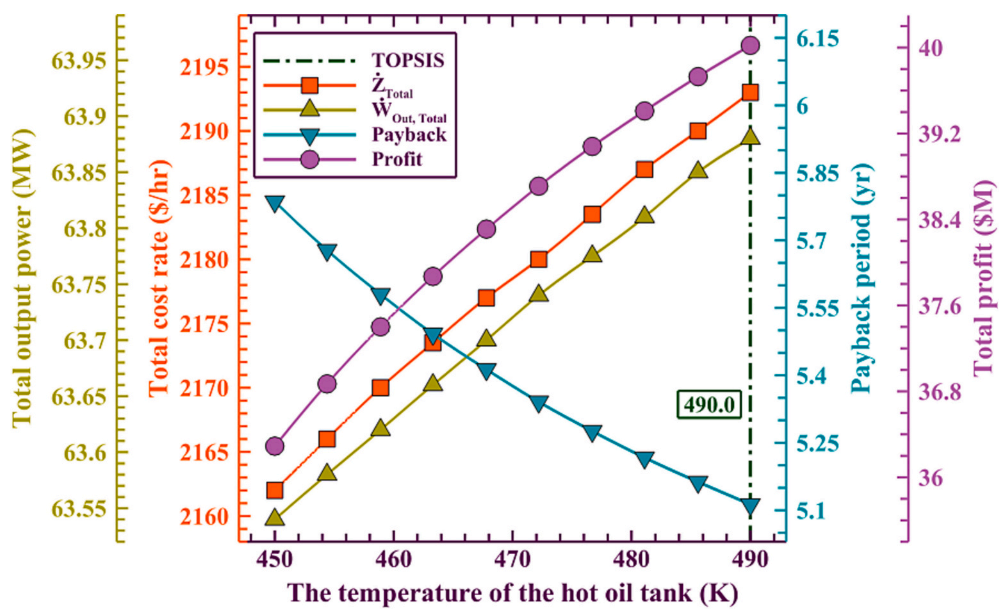

Fig. 11. The impact of the temperature of HOT on the total output power, total cost rate, payback period and total profit in the referenced CP-CAES system.

6.3. The Inlet pressure of the ST_1

The impact of the inlet pressure of ST_1 on the functionality of the referenced CP-CAES system is presented in Figs. 12 and 13. With increasing the pressure of the ST_1, the pressure of the ST_2 also goes up. As pressures are related to each other and they make a ratio. Pressure growth in STs results in increasing their expansion rate and consequently their power production. Increasing the pressure of the STs also results in higher compression ratio of the OP since its working pressure goes up. Totally with higher pressure of the STs the power out of the ORC cycle increases which leads to raising RTE, ERTE, and Imp_{Elec}. The temperature of the COT depends on the amount of heat exchanged in the SHs, Evap and the Eco as the inlet fluid to the COT passes through all these components. With increasing the pressure of the STs, the pressure and temperature of the fluid in the heat exchangers of the ORC cycle, and as a result pressure and temperature of the COT increase which lead to a slight increase in the power consumption of the ACs. With increasing the temperature of the COT, the temperature difference between HOT and COT decreases as the temperature of the HOT is considered to be unchanged. So, according to the energy balance equation, the oil's mass rate in the cycle is expected to raise to have the same rate of heat recovered by the oil in the cooler train. The increase in rate of the oil and higher expansion and compression rate in STs and OP, respectively, result in higher cost rate. The profit of the system goes up as the system's power out is rising and the price of the sold electricity to the network is higher than the expenses of the maintenance and purchasing of the components. Fig. 13 shows that the payback of the system has an optimal point from the tradeoff of the power out and the cost rate of the system. The optimum point is located close to the TOPSIS.

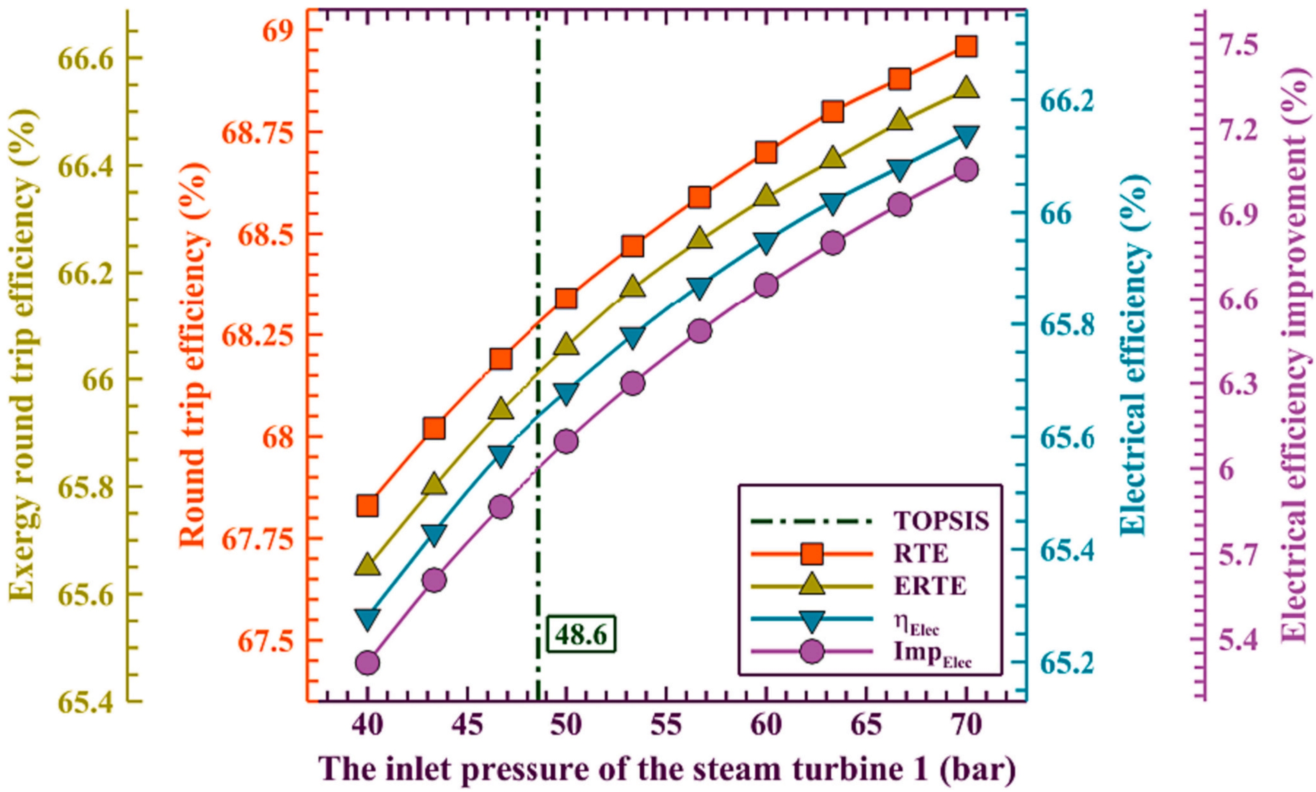

Fig. 12. The impact of the pressure of ST_1 on the RTE, ERTE, η_{Elec} and Imp_{Elec} in the referenced CP-CAES system.

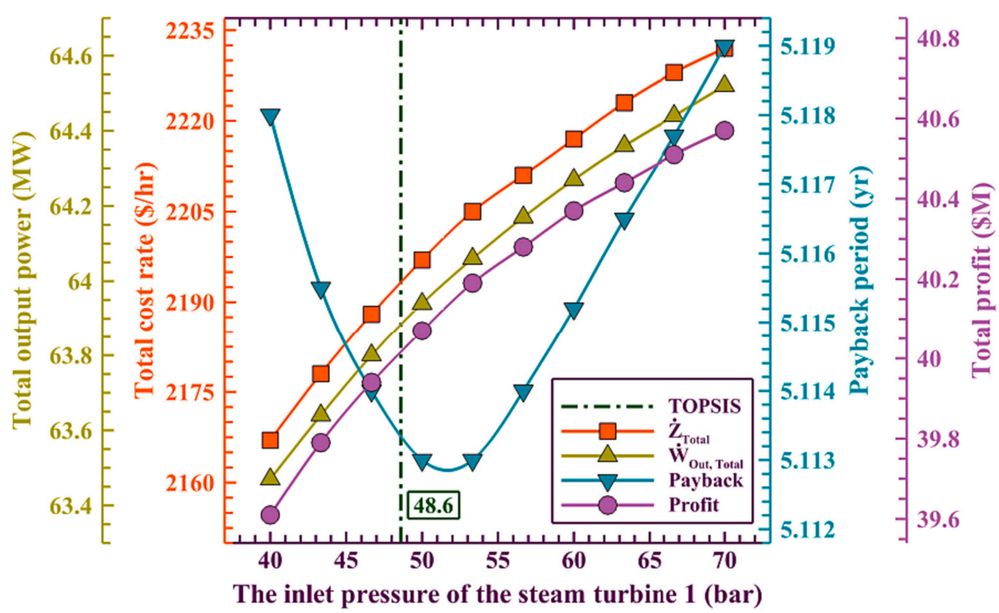

Fig. 13. The impact of the pressure of ST_1 on the total output power, total cost rate, payback period and total profit in the referenced CP-CAES system.

6.4. The pressure ratio of the reheat

The impact of the pressure ratio of the reheat on the functionality of the referenced CP-CAES system is presented in Figs. 14 and 15. The inlet pressure of the ST_1 and ST_2 are correlated with a ratio. In Figs. 14 and 15, the range of the ratio of the pressure of ST_2 to that for the ST_1 varies from 0.55 to 0.9. It can be seen that all the efficiency values shown in Fig. 14 have the same behavior as the power out of the system represented in Fig. 15. At first with increasing the pressure ratio, power generation of the system rises. However, improving the pressure ratio greater than 0.67 leads to output power reduction. Ultimate system's cost rate has a downward trend with increasing the pressure ratio. The effect of reducing the total cost rate on the total profit compared to decreasing the power out of the system is higher. As a result, the profit goes up with increasing the pressure ratio and the minimum payback of the system happens at the highest-pressure ratio.

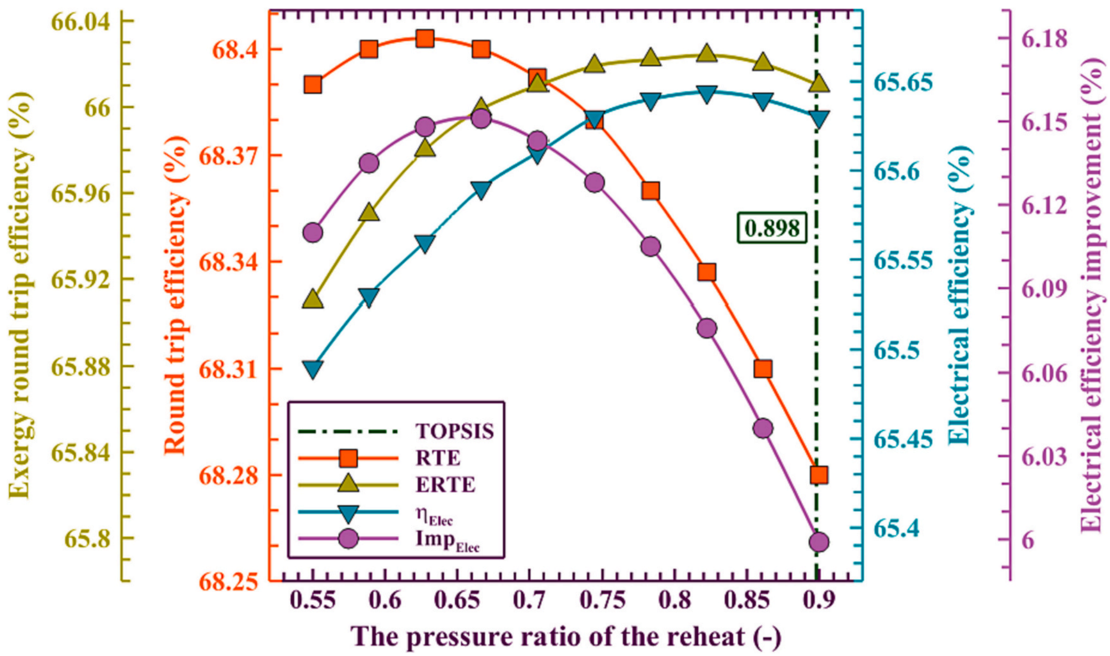

Fig. 14. The impact of the pressure ratio of the reheat on the RTE, ERTE, η_{Elec} and Imp_{Elec} in the referenced CP-CAES system.

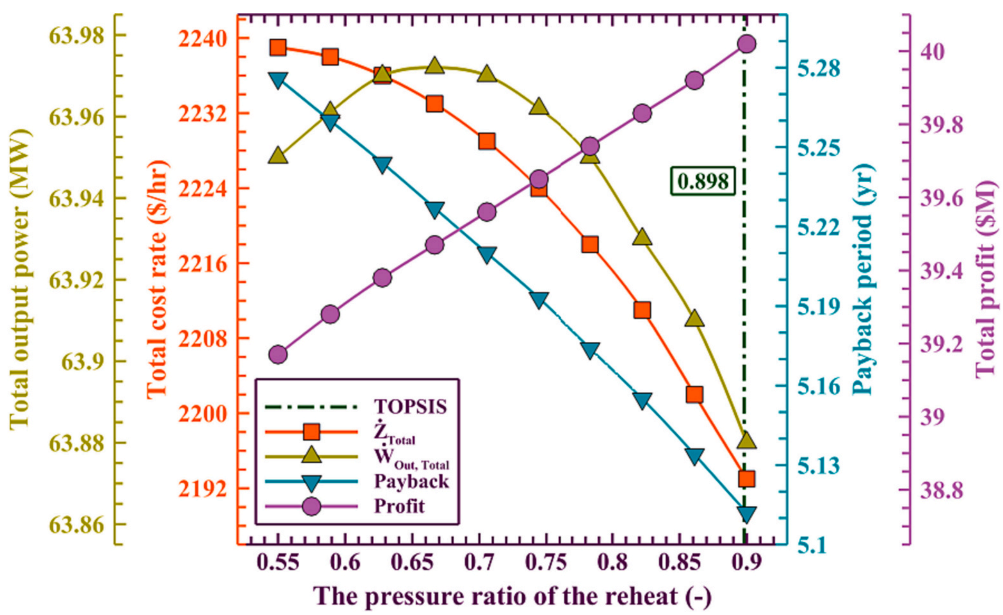

Fig. 15. The impact of the pressure ratio of the reheat on the total output power, total cost rate, payback period and total profit in the referenced CP-CAES system.

6.5. The inlet temperature of the ATs

The impact of AT's inlet temperature on the functionality of the referenced CP-CAES system is presented in Figs. 16 and 17. The inlet temperature of the ATs is a vital parameter in determining the total out power of the system. With raising the temperature of the inlet air to the ATs, the amount of the produced power by them goes up. In addition, the needed power in HTESs rises with increasing the temperature. The increase in the needed power of the HTESs can be justified according to the energy balance equation. As the temperature variation between the in and out fluids to the HTESs goes up the rate of the heat exchange in the HTESs increases. Therefore, higher inlet temperature of the inlet fluid to the ATs results in increasing both in and out total powers of the system. However, the growth in output power is more than increase in the inlet power to the system and as a result RTE, ERTE and η_{Elec} go up with increasing the temperature of the ATs. Fig. 16 displays that the total cost rate has an upward trend. The reason is that the size and as a result the cost of some components like ATs and HTESs increases. The optimum value of the payback of the system happens at a temperature around 1290 K. For temperatures lower than 1290 K the profit gained from selling the produced electricity of the system to the network is higher than the expenses of maintenance and component purchasing. As a result, the profit has an upward trend and payback of the system decreases. Increasing the temperature higher than the optimum value is not meaningful as it results in a reduction in profit and increasing the payback of the system. The best temperature is shown in Fig. 17 which is equal to 1383 K.

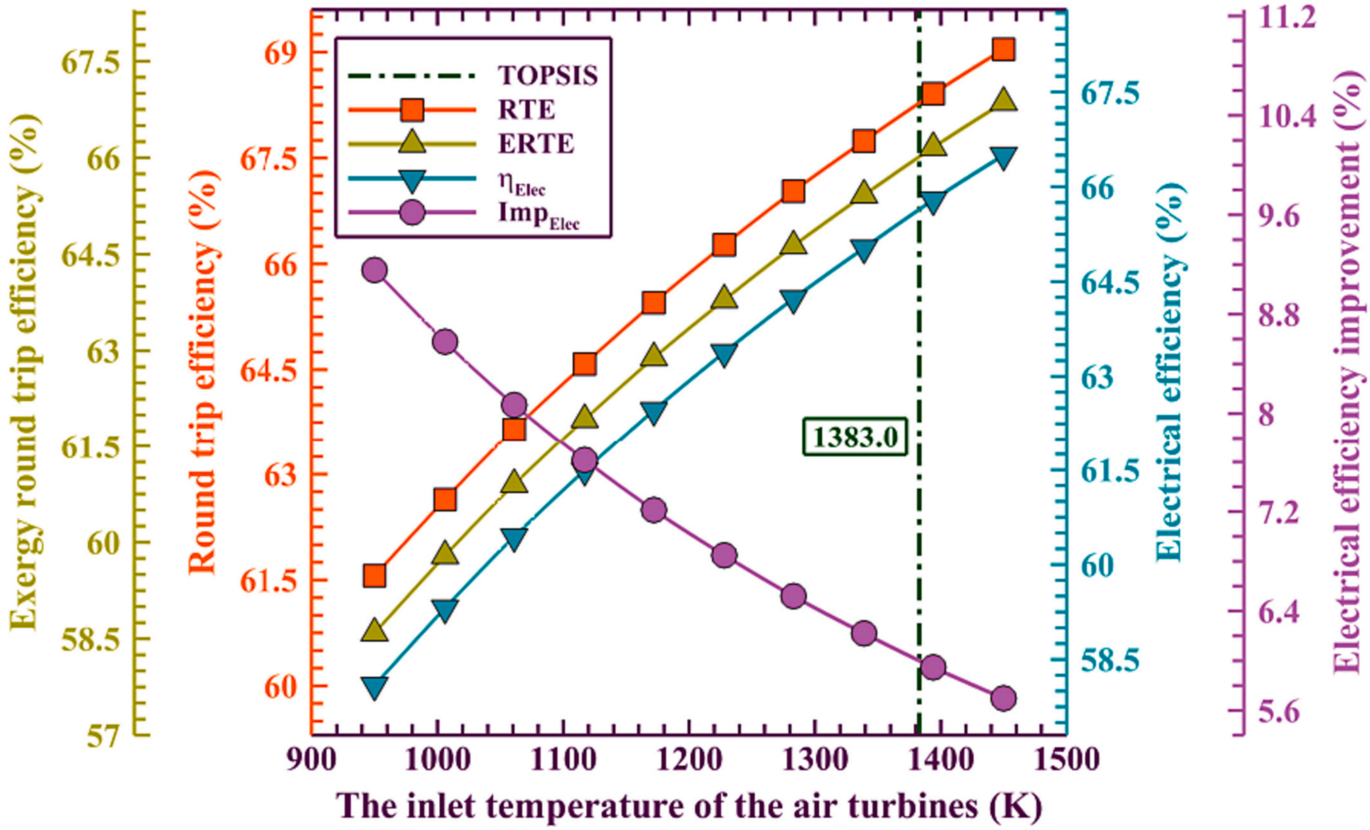

Fig. 16. The impact of the inlet temperature of AT on the RTE, ERTE, η_{Elec} and Imp_{Elec} in the referenced CP-CAES system.

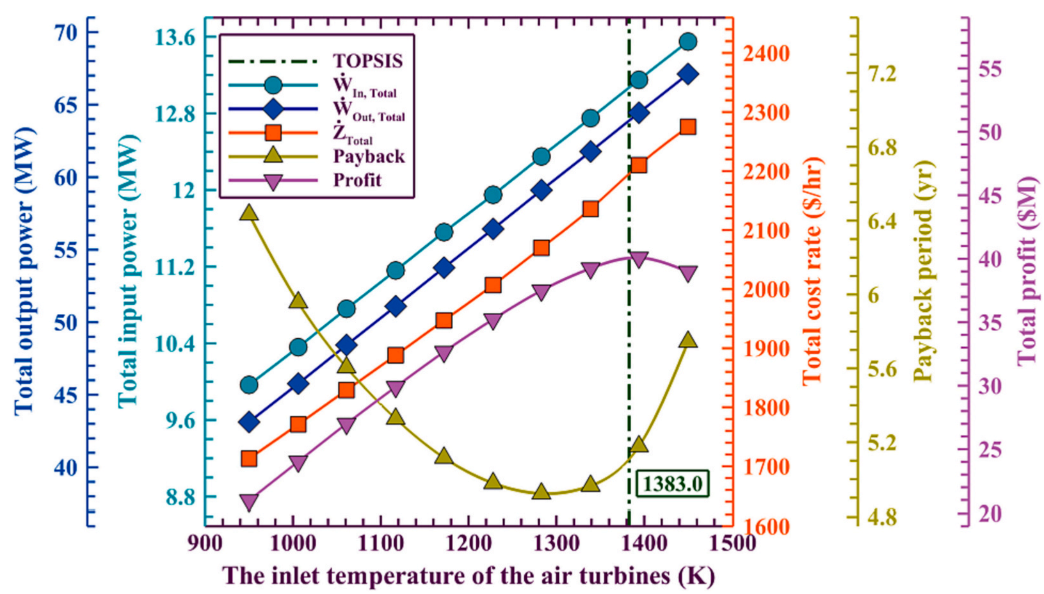

Fig. 17. The impact of the inlet temperature of AT on the total output power, total input power, total cost rate, payback period and total profit in the referenced CP-CAES system.

6.6. The charging period

The charging period impact on the functionality of the referenced CP-CAES system is represented in Fig. 18. Regarding the mass balance equation, the multiplication of the charging period and working fluid mass rate in charging process, is equivalent to the multiplication of the discharging time with the mass rate of the fluid in discharging process. Considering a constant value for mass rate of the charging process and the discharging period, increasing the charging time leads to a growth in the discharging mass rate. So, the mass rate in the HTESs and ATs as well as the mass rate of the outlet oil from HOT increases. According to the energy balance equation, increasing the mass rate of oil in the cooling loop causes the mass rate of the working fluid of ORC cycle to goes up. All in all, with raising the charging period the mass rate of the discharging processes goes up. Higher rate of fluid in Ats and STs results in higher power out of the CAES and the ORC cycles, respectively. Thus,

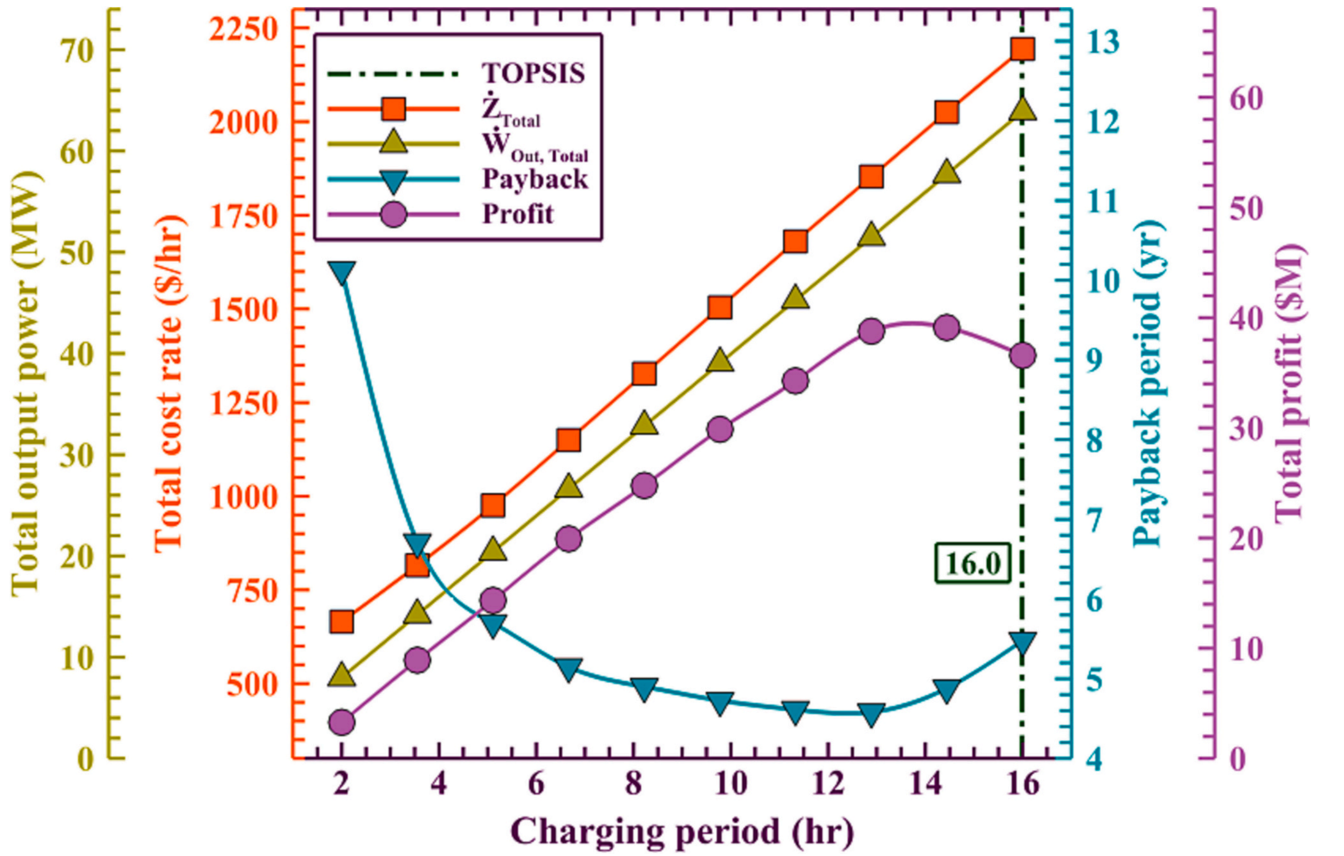

Fig. 18. The impact of charging period on the total output power, total cost rate, payback period and total profit in the referenced CP-CAES system.

the total power out of the system has an upward trend in Fig. 18. On the other hand, with increasing the mass rate of the fluid flowing into the components, their sizes need to be larger. So, the cost of purchasing the components like ATs, STs and heat exchangers in the cooling loop rises. Although the system's total cost rate increases, ultimate profit of the system has a growing trend. It is because of the higher impact of the boost in power out of the system on the total profit compared to the growth of the ultimate cost rate. With increasing the profit of the system, the payback period decreases, and its optimal value happens at high values of charging period.

6.7. The discharging period

The discharging period impact on the functionality of the system is shown in Fig. 19. Considering the mass rate of the charging process and the charging period remains constant, increasing discharging time causes the mass flow rate of the discharging processes to decrease. With decreasing the mass flow rate of the fluid flowing in the ATs and STs, the total power out of the system decreases. Components with smaller sizes are needed to handle the smaller mass rate of the working fluid. Consequently, the costs of purchasing the components decrease. At high discharging periods, the effect of reduction in power out of the system is much larger than that for reduction in total cost rate. So, as illustrated in Fig. 19, the ultimate profit of the system decreases, and the payback period goes up with increasing the discharging period. The optimum point of the system's payback period is located at low discharging time values near the TOPSIS, 2.15 h.

7. Comparative study

As previously stated, most of the CAES systems studied in the literature have used constant volume tanks for compressed air storage. The use of constant volume tanks has several disadvantages that affect the thermodynamic and economic performance of the system. In this regard, in this section, the proposed energy storage system has been modeled using a constant volume and a constant pressure tank and the results are compared in order to provide a better understanding of the advantages of the proposed system. To obtain an accurate comparison, two systems have been modeled with identical design conditions. It should be noted that for the system with constant volume tank, the charge to discharge pressure ratio is considered to be equal to 3. The thermodynamic, economic and exergoeconomic results of both systems are given in Tables 10 and 12.

Based on the results presented in Tables 10 and 12, the thermodynamic and economic performance of the proposed CP-CAES system is better than the CV-CAES system. Because the total power output, η_{Elec}, RTE and ERTE of the proposed CP-CAES system have been improved, 16.24 %, 2.59 %, 1.95 % and 2.50 %, respectively. On the other hand, the storage volume of the CV-CAES system is 1618 m^3 (52.53 %) higher than that for CP-CAES system. It is due to the fact that in CV-CAES system a part of the air stored in the tank is not released and remains in the tank as a dead volume. Improving the thermodynamic performance of the CP-CAES system results in enhancing the net profit and decreasing the payback period of the system. The net profit of the system increases from $ 32.92 M to $ 40.02 M and the payback period decreases from 5.34 to 5.11 years.

8. Conclusions and future works

The current study focuses on designing a CAES system with the main goal of enhancing the overall performance by minimizing exergy destruction through utilizing a constant pressure tank. The proposed design strives to attain the stated objective by removing the need for a regulator valve and maximizing the utilization of all the energy stored in

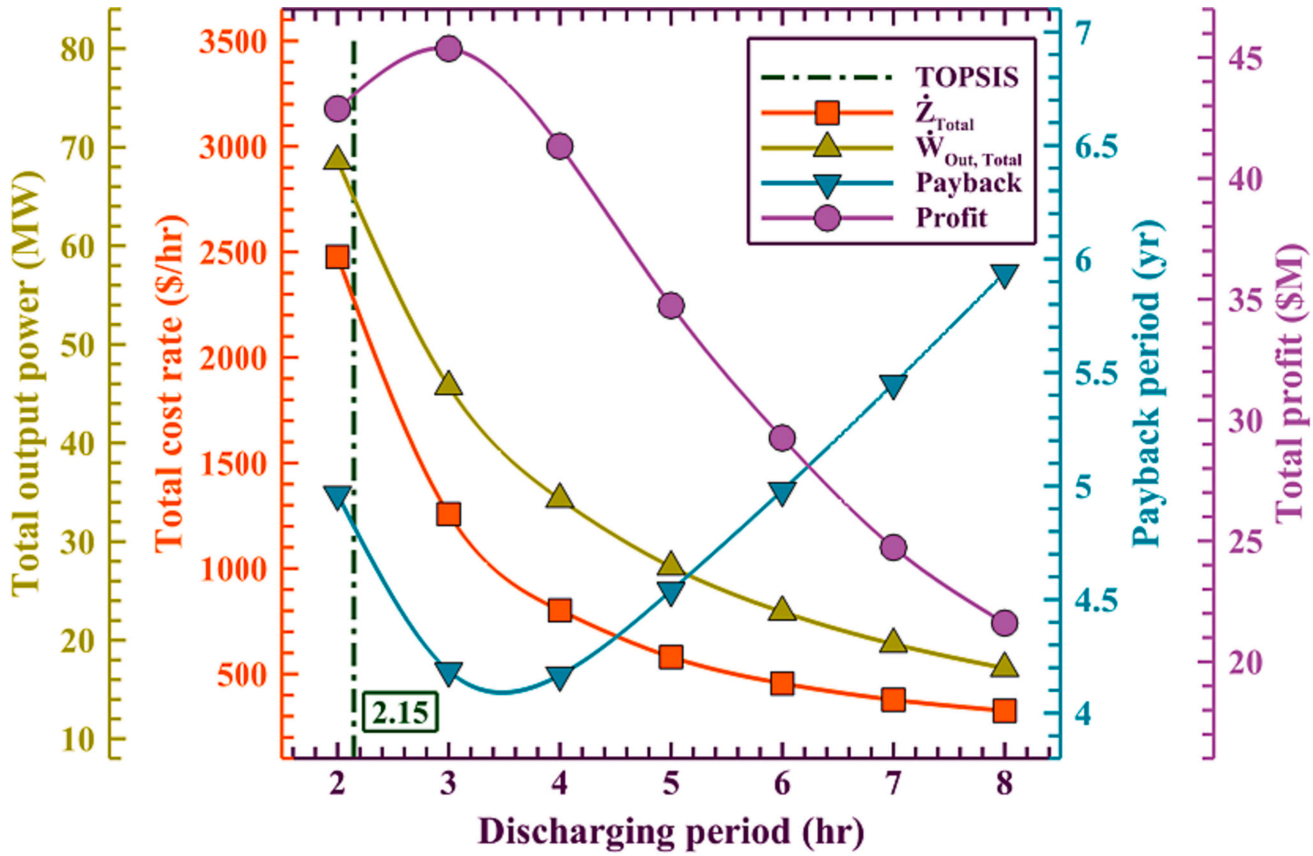

Fig. 19. The impact of discharging period on the total output power, total cost rate, payback period and total profit in the referenced CP-CAES system.

Table 12
The outcomes of energy, exergy, economic, and exergoeconomic analyses for the referenced CV-CAES system.

Parameter	Unit	Value	Parameter	Unit	Value
cp_{Total}	$/GJ	19.64	RTE	%	66.97
DPP	yr	5.338	TIC	$M	24.08
$ERTE$	%	64.4	Total profit	$M	32.92
η_{elec}	%	63.9	$TSED$	MJ/ m^3	57.24
η_{En}^{WHR}	%	14.31	V_{CAV}	m^3	4698
η_{Ex}^{WHR}	%	49.43	V_{COT}	m^3	759.1
Ex_d^{Total}	MWh	65.287	V_{HOT}	m^3	856
$LCOE$	$/MWh	194.0	$\dot{W}_{AC_1}$	kW	1103
$\dot{Q}_{C_1}$	kW	697	$\dot{W}_{AC_2}$	kW	1348
$\dot{Q}_{C_2}$	kW	1348	$\dot{W}_{AC_3}$	kW	1348
$\dot{Q}_{C_3}$	kW	1348	$\dot{W}_{AT_1}$	kW	17,114
$\dot{Q}_{Eco}$	kW	2351	$\dot{W}_{AT_2}$	kW	17,114
$\dot{Q}_{Evap}$	kW	14,815	$\dot{W}_{AT_3}$	kW	17,114
$\dot{Q}_{HHX}$	kW	345.3	$\dot{W}_{HT}$	kW	–
$\dot{Q}_{HTES_1}$	kW	17,628	$\dot{W}_{HTES_1}$	kW	2630
$\dot{Q}_{HTES_2}$	kW	17,114	$\dot{W}_{HTES_2}$	kW	2553
$\dot{Q}_{HTES_3}$	kW	17,114	$\dot{W}_{HTES_3}$	kW	2553
$\dot{Q}_{IHX}$	kW	1937	$\dot{W}_{OP}$	kW	126.1
$\dot{Q}_{Rec}$	kW	35,760	$\dot{W}_{ST_1}$	kW	353.8
$\dot{Q}_{SH_1}$	kW	7428	$\dot{W}_{ST_2}$	kW	3020
$\dot{Q}_{SH_2}$	kW	674.5	$\dot{W}_{TEG}$	kW	369.2
$\dot{Q}_{TEG}$	kW	22,020	$\dot{W}_{WP}$	kW	–

compressed air. The second objective of the CP-CAES system is to enhance the storage pressure within the constant pressure tanks, overcoming previous limitations observed in comparable constant pressure systems. The third objective is to independently harness the heat recovery unit, facilitating more effective control of the storage systems, particularly during the discharge phase. The referenced CP-CAES system is completely evaluated from the energy, exergy, economy, and exergoeconomic (4E) perspectives to provide all-encompassing elucidation of the key features. By implementing a multi-criteria optimization, the ideal quantities for the referenced CP-CAES system are presented considering a trade-off between the thermodynamic and economic aspects. The main outcomes of this study are:

- The referenced CP-CAES system can store 209 MWh of cheap network electricity in the form of heat and compressed air through off-peak periods. In times of peak period, the stored energy is utilized to produce 137.2 MWh electrical power for peak shaving purposes. According to the achieved findings from thermodynamic evaluation, the η_{Elec}, RTE, and ERTE of the system are 65.63 %, 68.28 %, and 66.01 %, respectively.
- To investigate the main cause of irreversibility in the referenced CP-CAES system, a Grassmann exergy diagram is provided. The overall amount of exergy destruction is 69.52 MWh, with a considerable portion attributed to HTESs.
- The performance of the system is further analyzed parametrically to identify key parameters that have a considerable effect on the functionality of the system. The results indicate that the pressure of CAV, the input pressure to ST_1, the reheating pressure ratio of the thermal recovery cycle, the inlet temperature to AT, the temperature of HOT, charge, and discharge periods are the most important factors, which are all decision variables considered for optimization.
- Considering the findings achieved from the economic evaluation done for California, USA, the investment cost required to construct the designed power plant is estimated to be $ 27.68 M. In addition, the overall profit and payback period of the system are estimated to be $ 40.02 M and 5.113 years, accordingly. Regarding the exergoeconomic evaluation, the total cost of products (cp_{Total}), and

levelized cost of the electricity (LCOE) are 21.15 $/GJ and 190.4 $/MWh, respectively.
- The ultimate power production of the system and its return on investment are estimated by the ANN algorithm with high accuracy to eliminate utilizing the simulation code directly when optimizing the system. The values of energy and exergy efficiencies of the WHR system are 14.31 % and 49.43 %, respectively.

8.1. Applications and limitations

The proposed system holds potential for diverse applications. It can serve as a reliable backup power source for critical industries during periods of power disruptions, offering resilience to their operations. Additionally, it exhibits the capacity to stabilize the electrical grid by swiftly discharging energy to meet peak demand or grid fluctuations. Furthermore, the system's versatility extends to integration with renewable energy sources such as wind and solar, enabling the storage of excess energy for release during high-demand periods when these renewables are less productive. Importantly, this system operates without any reliance on fossil fuels and exclusively draws surplus electricity during off-peak periods, resulting in a minimal environmental footprint. The ecological advantages of this system render it particularly suitable for regions or countries committed to zero emissions and incentivized by carbon credits, enhancing its economic appeal.

Nevertheless, the system is not devoid of limitations. The prospect of expanding its capacity to generate additional power for increased profitability is conceivable, but such an expansion entails higher demand for synthetic oil for waste heat recovery, a costly endeavor that significantly impacts the overall investment cost. The limitations of synthetic oil use in high capacities must be acknowledged. Furthermore, scaling up the system necessitates HTES units with larger storage capacities. However, these units have inherent size limitations, resulting in constraints on storage capacity. Moreover, metallurgical constraints impose limits on the high temperature achievable with HTES, as elevating this temperature substantially is unfeasible. Conversely, raising the low temperature threshold is similarly restricted, as it inflates both the occupied volume and acquisition cost of the HTES unit. As elucidated in Section 3.2.3, the economic viability of storage systems is intrinsically tied to the price dynamics of electricity purchase and sale. Consequently, the optimal use of the proposed system is in regions characterized by dynamic electricity pricing, where the acquisition of cost-effective electricity and its resale at higher rates can yield a commendable return on investment.

8.2. Outlooks and future studies

The proposed system is composed of several distinct sub-systems, and enhancing the performance of each of these components holds the potential to yield overall system improvements. Notably, the waste heat recovery unit assumes a pivotal role in the entire energy storage system, warranting an in-depth assessment of various waste heat recovery systems. It is advisable to explore alternative systems such as Kalina, Goswami, and Thermophotovoltaic generators to evaluate and compare their performance against the ORC system. Given the prohibitively high cost of synthetic oils, especially when deployed at larger capacities, a comprehensive analysis of diverse oils from both thermodynamic and economic perspectives presents an attractive avenue to mitigate investment costs and, consequently, elevate the economic viability of the system. Furthermore, investigating the replacement of the TEG unit with an alternative heat recovery system like Thermophotovoltaic generators, which may offer improved efficiency, represents another promising approach to enhance the overall system performance.

CRediT authorship contribution statement

Mohammad Hossein Nabat: Conceptualization, Methodology, Investigation, Software, Visualization, Validation, Formal analysis, Project administration, Writing – review & editing. **Mehran Habibzadeh:** Conceptualization, Methodology, Investigation, Software, Visualization, Formal analysis, Writing – original draft. **Ali Sulaiman Alsagri:** Conceptualization, Writing – review & editing. **Ahmad Arabkoohsar:** Conceptualization, Methodology, Supervision, Writing – review & editing.

Declaration of competing interest

The authors do not see any conflicts of interest.

Data availability

No data was used for the research described in the article.

References

[1] M. Momeni, A. Fartaj, Numerical thermal performance analysis of a PCM-to-air and liquid heat exchanger implementing latent heat thermal energy storage, J. Energy Storage. 58 (2023), 106363, https://doi.org/10.1016/J.EST.2022.106363.
[2] L. Zhang, L. Liu, C. Zhang, X. He, Y. Zhang, T. Yang, Performance analysis of an adiabatic compressed air energy storage system with a pressure regulation inverter-driven compressor, J. Energy Storage. 43 (2021), 103197, https://doi.org/10.1016/J.EST.2021.103197.
[3] S.M. Babaei, M.H. Nabat, F. Lashgari, M.Z. Pedram, A. Arabkoohsar, Thermodynamic analysis and optimization of an innovative hybrid multi-generating liquid air energy storage system, J. Energy Storage. 43 (2021), 103262, https://doi.org/10.1016/j.est.2021.103262.
[4] A. Daneshvar Garmroodi, F. Nasiri, F. Haghighat, Optimal dispatch of an energy hub with compressed air energy storage: a safe reinforcement learning approach, J. Energy Storage. 57 (2023), 106147, https://doi.org/10.1016/J.EST.2022.106147.
[5] A.R. Razmi, A.R. Hanifi, M. Shahbakhti, Design, thermodynamic, and economic analyses of a green hydrogen storage concept based on solid oxide electrolyzer/fuel cells and heliostat solar field, Renew. Energy 215 (2023), 118996, https://doi.org/10.1016/J.RENENE.2023.118996.
[6] S. Sharifi, A.R. Razmi, M.H. Nabat, J.J. Liu, A. Arabkoohsar, M. Shahbakhti, Power-to-X, Futur. Grid-Scale Energy Storage Solut. Mech. Chem. Technol. Princ, 2023, pp. 621–646, https://doi.org/10.1016/B978-0-323-90786-6.00003-0.
[7] S. Qing, Y. Wang, X. Wen, J. Zhong, X. Gou, S. Tang, Optimal working-parameter analysis of an ejector integrated into the energy-release stage of a thermal-storage compressed air energy storage system under constant-pressure operation: a case study, Energ. Conver. Manage. 247 (2021), 114715, https://doi.org/10.1016/J.ENCONMAN.2021.114715.
[8] A.R. Razmi, S.M. Alirahmi, M.H. Nabat, E. Assareh, M. Shahbakhti, A green hydrogen energy storage concept based on parabolic trough collector and proton exchange membrane electrolyzer/fuel cell: thermodynamic and exergoeconomic analyses with multi-objective optimization, Int. J. Hydrogen Energy 47 (2022) 26468–26489, https://doi.org/10.1016/J.IJHYDENE.2022.03.021.
[9] L. Chen, L. Zhang, Y. Wang, M. Xie, H. Yang, K. Ye, S. Mohtaram, Design and performance evaluation of a novel system integrating water-based carbon capture with adiabatic compressed air energy storage, Energ. Conver. Manage. 276 (2023), 116583, https://doi.org/10.1016/j.enconman.2022.116583.
[10] A. Razmi, M. Soltani, M. Torabi, Investigation of an efficient and environmentally-friendly CCHP system based on CAES, ORC and compression-absorption refrigeration cycle: energy and exergy analysis, Energ. Conver. Manage. 195 (2019) 1199–1211, https://doi.org/10.1016/J.ENCONMAN.2019.05.065.
[11] H.R. Rahbari, A. Arabkoohsar, M. Sadi, Tri-generating compressed air energy storage, Futur. Grid-Scale Energy Storage Solut. (2023) 309–343, https://doi.org/10.1016/B978-0-323-90786-6.00015-7.
[12] S. Chen, H.R. Rahbari, A. Arabkoohsar, T. Zhu, G. Chen, Compressed air energy storage system, Futur. Grid-Scale Energy Storage Solut. (2023) 269–308, https://doi.org/10.1016/B978-0-323-90786-6.00004-2.
[13] M. Ebrahimi, R. Carriveau, D.S.K. Ting, A. McGillis, Conventional and advanced exergy analysis of a grid connected underwater compressed air energy storage facility, Appl. Energy 242 (2019) 1198–1208, https://doi.org/10.1016/J.APENERGY.2019.03.135.
[14] Z. Wang, W. Xiong, D.S.K. Ting, R. Carriveau, Z. Wang, Conventional and advanced exergy analyses of an underwater compressed air energy storage system, Appl. Energy 180 (2016) 810–822, https://doi.org/10.1016/J.APENERGY.2016.08.014.
[15] P. Zhao, W. Xu, W. He, J. Wang, Z. Yan, Thermo-economic analysis of a hybrid system based on combined heat - isobaric compressed air energy storage and humidification dehumidification desalination unit, Appl. Therm. Eng. 219 (2023), 119536, https://doi.org/10.1016/J.APPLTHERMALENG.2022.119536.
[16] Z. Liu, X. Liu, S. Yang, K. Hooman, X. Yang, Assessment evaluation of a trigeneration system incorporated with an underwater compressed air energy

storage, Appl. Energy 303 (2021), 117648, https://doi.org/10.1016/J.APENERGY.2021.117648.
[17] H. Guo, Y. Xu, Y. Zhu, X. Zhang, Z. Yin, H. Chen, Coupling properties of thermodynamics and economics of underwater compressed air energy storage systems with flexible heat exchanger model, J. Energy Storage. 43 (2021), 103198, https://doi.org/10.1016/J.EST.2021.103198.
[18] Z. Wang, D.S.K. Ting, R. Carriveau, W. Xiong, Z. Wang, Design and thermodynamic analysis of a multi-level underwater compressed air energy storage system, J. Energy Storage. 5 (2016) 203–211, https://doi.org/10.1016/J.EST.2016.01.002.
[19] L.X. Chen, M.N. Xie, P.P. Zhao, F.X. Wang, P. Hu, D.X. Wang, A novel isobaric adiabatic compressed air energy storage (IA-CAES) system on the base of volatile fluid, Appl. Energy 210 (2018) 198–210, https://doi.org/10.1016/J.APENERGY.2017.11.009.
[20] L. Chen, Y. Wang, M. Xie, K. Ye, S. Mohtaram, Energy and exergy analysis of two modified adiabatic compressed air energy storage (A-CAES) system for cogeneration of power and cooling on the base of volatile fluid, J. Energy Storage. 42 (2021), 103009, https://doi.org/10.1016/J.EST.2021.103009.
[21] K.J. Rolland, T. Nitsche, M. Budt, C. Doetsch, Isobaric storage of compressed air: introduction of a novel concept based on phase change materials and pressure equalizing modules, J. Energy Storage. 61 (2023), 106778, https://doi.org/10.1016/J.EST.2023.106778.
[22] H. Wang, Z. Tong, X. Dong, W. Xiong, D.S.K. Ting, R. Carriveau, Z. Wang, Design and energy saving analysis of a novel isobaric compressed air storage device in pneumatic systems, J. Energy Storage. 38 (2021), 102614, https://doi.org/10.1016/j.est.2021.102614.
[23] S.M. Alirahmi, A.R. Razmi, A. Arabkoohsar, Comprehensive assessment and multi-objective optimization of a green concept based on a combination of hydrogen and compressed air energy storage (CAES) systems, Renew. Sustain. Energy Rev. 142 (2021), 110850, https://doi.org/10.1016/J.RSER.2021.110850.
[24] S.M. Alirahmi, S. Bashiri Mousavi, A.R. Razmi, P. Ahmadi, A comprehensive techno-economic analysis and multi-criteria optimization of a compressed air energy storage (CAES) hybridized with solar and desalination units, Energ. Conver. Manage. 236 (2021), 114053, https://doi.org/10.1016/j.enconman.2021.114053.
[25] P. Yin, F. Sardari, Process arrangement and multi-criteria study/optimization of a novel hybrid solar-geothermal scheme combined with a compressed air energy storage: application of different MOPSO-based scenarios, Energy 282 (2023), 128651, https://doi.org/10.1016/j.energy.2023.128651.
[26] T. Hai, M. Zoghi, K. Javaherdeh, 4E analysis and optimization of a biomass-fired waste-to-energy plant integrated with a compressed air energy storage system for the multi-generation purpose, Fuel 348 (2023), 128457, https://doi.org/10.1016/j.fuel.2023.128457.
[27] S.B. Mousavi, P. Ahmadi, A. Pourahmadiyan, P. Hanafizadeh, A comprehensive techno-economic assessment of a novel compressed air energy storage (CAES) integrated with geothermal and solar energy, Sustain. Energy Technol. Assessments. 47 (2021), 101418, https://doi.org/10.1016/J.SETA.2021.101418.
[28] S.M. Alirahmi, A. Ebrahimi-Moghadam, Comparative study, working fluid selection, and optimal design of three systems for electricity and freshwater based on solid oxide fuel cell mover cycle, Appl. Energy 323 (2022), 119545, https://doi.org/10.1016/J.APENERGY.2022.119545.
[29] A.R. Razmi, S. Sharifi, S. Vafaeenezhad, A.R. Hanifi, M. Shahbakhti, Modeling and microstructural study of anode-supported solid oxide fuel cells: experimental and thermodynamic analyses, Int. J. Hydrogen Energy (2023), https://doi.org/10.1016/J.IJHYDENE.2023.08.296.
[30] M.H. Nabat, S. Sharifi, A.R. Razmi, Thermodynamic and economic analyses of a novel liquid air energy storage (LAES) coupled with thermoelectric generator and Kalina cycle, J. Energy Storage. 45 (2022), 103711, https://doi.org/10.1016/J.EST.2021.103711.
[31] B. Kantharaj, S. Garvey, A. Pimm, Thermodynamic analysis of a hybrid energy storage system based on compressed air and liquid air, Sustain. Energy Technol. Assessments. 11 (2015) 159–164, https://doi.org/10.1016/j.seta.2014.11.002.
[32] Y. Li, H. Cao, S. Wang, Y. Jin, D. Li, X. Wang, Y. Ding, Load shifting of nuclear power plants using cryogenic energy storage technology, Appl. Energy 113 (2014) 1710–1716, https://doi.org/10.1016/j.apenergy.2013.08.077.
[33] H.R. Abbasi, H. Pourrahmani, Multi-objective optimization and exergoeconomic analysis of a continuous solar-driven system with PCM for power, cooling and freshwater production, Energ. Conver. Manage. 211 (2020), 112761, https://doi.org/10.1016/j.enconman.2020.112761.
[34] M. Nourpour, M.H. Khoshgoftar Manesh, Evaluation of novel integrated combined cycle based on gas turbine-SOFC-geothermal-steam and organic Rankine cycles for gas turbo compressor station, Energ. Conver. Manage. 252 (2022), 115050, https://doi.org/10.1016/j.enconman.2021.115050.
[35] Y.A. Cengel, M.A. Boles, M. Kanoglu, Thermodynamics an engineering approach, Ninth Edition, 2019. ISBN139789813157873.
[36] M.A. Kordlar, F. Heberle, D. Brüggemann, Thermo-economic evaluation of a tri-generation system driven by geothermal brine to cover flexible heating and cooling demand, Geothermics 110 (2023), 102678, https://doi.org/10.1016/J.GEOTHERMICS.2023.102678.
[37] M.A. Kordlar, F. Heberle, D. Brüggemann, Evaluation and optimization of the annual performance of a novel tri-generation system driven by geothermal brine in off-design conditions, Appl. Sci. 10 (2020) 6532, https://doi.org/10.3390/APP10186532.
[38] S. Mohtaram, W. Wu, Y. Aryanfar, Q. Yang, J.L. García Alcaraz, Introducing and assessment of a new wind and solar-based diversified energy production system intergrading single-effect absorption refrigeration, ORC, and SRC cycles, Renew. Energy 199 (2022) 179–191, https://doi.org/10.1016/j.renene.2022.08.069.
[39] M. Akbari Kordlar, S.M.S. Mahmoudi, F. Talati, M. Yari, A.H. Mosaffa, A new flexible geothermal based cogeneration system producing power and refrigeration, part two: the influence of ambient temperature, Renew. Energy 134 (2019) 875–887, https://doi.org/10.1016/J.RENENE.2018.11.082.
[40] S.M.S. Mahmoudi, M. Akbari Kordlar, A new flexible geothermal based cogeneration system producing power and refrigeration, Renew. Energy 123 (2018) 499–512, https://doi.org/10.1016/J.RENENE.2018.02.060.
[41] M.H. Nabat, M. Zeynalian, A.R. Razmi, A. Arabkoohsar, M. Soltani, Energy, exergy, and economic analyses of an innovative energy storage system; liquid air energy storage (LAES) combined with high-temperature thermal energy storage (HTES), Energ. Conver. Manage. 226 (2020), 113486, https://doi.org/10.1016/j.enconman.2020.113486.
[42] A. Bejan, G. (George) Tsatsaronis, M.J. Moran, Chapter 3: exergy analysis, in: Therm. Des. Optim, 1996.
[43] A. Habibollahzade, E. Gholamian, P. Ahmadi, A. Behzadi, Multi-criteria optimization of an integrated energy system with thermoelectric generator, parabolic trough solar collector and electrolysis for hydrogen production, Int. J. Hydrogen Energy 43 (2018) 14140–14157, https://doi.org/10.1016/J.IJHYDENE.2018.05.143.
[44] T.M. Tritt, M.A. Subramanian, Thermoelectric Materials, Phenomena, and Applications: A Bird's Eye View vol. 31, 2020.
[45] N. Nezamoddini, Y. Wang, Real-time electricity pricing for industrial customers: survey and case studies in the United States, Appl. Energy 195 (2017) 1023–1037, https://doi.org/10.1016/J.APENERGY.2017.03.102.
[46] S.M. Alirahmi, E. Assareh, N.N. Pourghassab, M. Delpisheh, L. Barelli, A. Baldinelli, Green hydrogen & electricity production via geothermal-driven multi-generation system: thermodynamic modeling and optimization, Fuel 308 (2022), 122049, https://doi.org/10.1016/J.FUEL.2021.122049.
[47] S. Wu, C. Zhou, E. Doroodchi, B. Moghtaderi, Techno-economic analysis of an integrated liquid air and thermochemical energy storage system, Energ. Conver. Manage. 205 (2020), 112341, https://doi.org/10.1016/J.ENCONMAN.2019.112341.
[48] C. Zheng, X. Qi, H. Yang, X. Yujie, C. Haisheng, D. Jianqiang, Discharging strategy of adiabatic compressed air energy storage system based on variable load and economic analysis, J. Energy Storage. 51 (2022), 104403, https://doi.org/10.1016/j.est.2022.104403.
[49] A.R. Razmi, M. Janbaz, Exergoeconomic assessment with reliability consideration of a green cogeneration system based on compressed air energy storage (CAES), Energ. Conver. Manage. 204 (2020), 112320, https://doi.org/10.1016/j.enconman.2019.112320.
[50] Ö. Köse, Y. Koç, H. Yağlı, Is Kalina cycle or organic Rankine cycle for industrial waste heat recovery applications? A detailed performance, economic and environment based comprehensive analysis, Process. Saf. Environ. Prot. 163 (2022) 421–437, https://doi.org/10.1016/j.psep.2022.05.041.
[51] R. Turton, R.C. Bailie, W.B. Whiting, J.A. Shaeiwitz, Analysis, Synthesis and Design of Chemical Processes, Pearson Education, 2008.
[52] M. Ebadollahi, H. Rostamzadeh, M.Z. Pedram, H. Ghaebi, M. Amidpour, Proposal and assessment of a new geothermal-based multigeneration system for cooling, heating, power, and hydrogen production, using LNG cold energy recovery, Renew. Energy 135 (2019) 66–87, https://doi.org/10.1016/j.renene.2018.11.108.
[53] N. Khani, M.H. Khoshgoftar Manesh, V.C. Onishi, 6E analyses of a new solar energy-driven polygeneration system integrating CO2 capture, organic Rankine cycle, and humidification-dehumidification desalination, J. Clean. Prod. 379 (2022), 134478, https://doi.org/10.1016/j.jclepro.2022.134478.
[54] M.H. Nabat, M. Soltani, A.R. Razmi, J. Nathwani, M.B. Dusseault, Investigation of a green energy storage system based on liquid air energy storage (LAES) and high-temperature concentrated solar power (CSP): energy, exergy, economic, and environmental (4E) assessments, along with a case study for San Diego, US, Sustain. Cities Soc. 75 (2021), 103305, https://doi.org/10.1016/J.SCS.2021.103305.
[55] S.M. Alirahmi, A. Ebrahimi-Moghadam, Comparative study, working fluid selection, and optimal design of three systems for electricity and freshwater based on solid oxide fuel cell mover cycle, Appl. Energy 323 (2022), 119545, https://doi.org/10.1016/j.apenergy.2022.119545.
[56] W. Wu, S. Xie, J. Tan, T. Ouyang, An integrated design of LNG cold energy recovery for supply demand balance using energy storage devices, Renew. Energy 183 (2022) 830–848, https://doi.org/10.1016/j.renene.2021.11.066.
[57] S.M. Alirahmi, E. Assareh, A. Chitsaz, S. Ghazanfari Holagh, S. Jalilinasrabady, Electrolyzer-fuel cell combination for grid peak load management in a geothermal power plant: power to hydrogen and hydrogen to power conversion, Int. J. Hydrogen Energy (2021), https://doi.org/10.1016/j.ijhydene.2021.05.082.
[58] Y. Aryanfar, S. Mohtaram, J.L. García Alcaraz, H.G. Sun, Energy and exergy assessment and a competitive study of a two-stage ORC for recovering SFGC waste heat and LNG cold energy, Energy 264 (2023), 126191, https://doi.org/10.1016/j.energy.2022.126191.
[59] N. Chitgar, M.A. Emadi, Development and exergoeconomic evaluation of a SOFC-GT driven multi-generation system to supply residential demands: electricity, fresh water and hydrogen, Int. J. Hydrogen Energy 46 (2021) 17932–17954, https://doi.org/10.1016/j.ijhydene.2021.02.191.
[60] S.M. Alirahmi, A. Behzadi, P. Ahmadi, S. Sadrizadeh, An innovative four-objective dragonfly-inspired optimization algorithm for an efficient, green, and cost-effective waste heat recovery from SOFC, Energy 263 (2023), 125607, https://doi.org/10.1016/j.energy.2022.125607.
[61] Z. Gao, L. Guo, W. Ji, H. Xu, B. An, J. Wang, Thermodynamic and economic analysis of a trigeneration system based on liquid air energy storage under different

operating modes, Energ. Conver. Manage. 221 (2020), 113184, https://doi.org/10.1016/J.ENCONMAN.2020.113184.
[62] S. Bashiri Mousavi, M.H. Nabat, A.R. Razmi, P. Ahmadi, A comprehensive study and multi-criteria optimization of a novel sub-critical liquid air energy storage (SC-LAES), Energ. Conver. Manage. 258 (2022), 115549, https://doi.org/10.1016/J.ENCONMAN.2022.115549.
[63] M.H. Nabat, A.R. Razmi, S. Sharifi, A. Arabkoohsar, M. Shahbakhti, Liquid air energy storage, in: Futur. Grid-Scale Energy Storage Solut. Mech. Chem. Technol. Princ, 2023, pp. 345–408, https://doi.org/10.1016/B978-0-323-90786-6.00016-9.
[64] L. Chen, D. Cheng, P. Tang, D. Yao, Combination of compressed air energy storage and Kalina 11 cycles for sustainable energy provision; energy, exergy, and economic analysis, Int. J. Energy Res. 45 (2021) 19962–19984, https://doi.org/10.1002/ER.7071.
[65] A. Sadreddini, M. Fani, M. Ashjari Aghdam, A. Mohammadi, Exergy analysis and optimization of a CCHP system composed of compressed air energy storage system and ORC cycle, Energ. Conver. Manage. 157 (2018) 111–122, https://doi.org/10.1016/J.ENCONMAN.2017.11.055.